Flux globalization based well-balanced central-upwind scheme for one-dimensional blood flow models

Shaoshuai Chu[1] · Alexander Kurganov[2]

Abstract

We develop a new second-order well-balanced central-upwind scheme for one-dimensional blood flow models. The proposed scheme is based on a flux globalization approach, which helps to develop a high-resolution and robust method capable of preserving both "man-at-eternal-rest" (zero-velocity) and "living-man" (non-zero velocity) steady-state solutions. We demonstrate the performance of the designed schemes on several numerical examples.

1 Introduction

The goal of this paper is to develop a high-resolution and robust well-balanced (WB) numerical method for one-dimensional (1-D) blood flow models in arteries. Such models have been extensively used to study wave propagation phenomena in arteries of the human cardiovascular system; see, e.g., [9, 22].

✉ Alexander Kurganov
alexander@sustech.edu.cn

Shaoshuai Chu
chuss2019@mail.sustech.edu.cn

[1] Department of Mathematics, Southern University of Science and Technology, Shenzhen 518055, China

[2] Department of Mathematics, SUSTech International Center for Mathematics and Guangdong Provincial Key Laboratory of Computational Science and Material Design, Southern University of Science and Technology, Shenzhen 518055, China

A well-established nonconservative formulation for the 1-D blood flow in human arteries takes the following form (see, e.g., the review paper [24] and references therein):

$$\begin{cases} A_t + Q_x = 0, \\ Q_t + \left(\hat{\alpha} \dfrac{Q^2}{A} \right)_x + \dfrac{A}{\rho} p_x = f, \end{cases} \tag{1.1}$$

where $A(x, t) = \pi r^2(x, t)$ is the cross-sectional area of the vessel or tube at spatial position x and time t with $r(x, t) > 0$ being the radius; $Q(x, t) = A(x, t)u(x, t)$ is the discharge with $u(x, t)$ representing the average velocity of the flow; the Coriolis coefficient $\hat{\alpha}$ is the momentum-flux correction that, in general, depends on the assumed velocity profile, but in this paper taken $\hat{\alpha} \equiv 1$, which corresponds to a flat velocity profile; $\rho > 0$ is the constant blood density; and $p(x, t) > 0$ is the average internal pressure. Finally, $f(x, t)$ is the friction force per unit length modeled by

$$f(x, t) = -\alpha(x)u(x, t), \tag{1.2}$$

where the viscous resistance $\alpha(x) > 0$ is a prescribed function.

In order to close the system (1.1)–(1.2), one needs to complete it with a pressure law linking the average pressure $p(x, t)$ with the cross-sectional area $A(x, t)$. In the present work, we use a simple elastic tube law that describes the elastic behavior of the arterial wall:

$$p = p_{\text{ext}} + \frac{\kappa}{\sqrt{\pi}} \left(\sqrt{A} - \sqrt{B} \right), \tag{1.3}$$

where the external pressure p_{ext} is assumed to be constant, the constant κ stands for the arterial stiffness, and $B(x) = \pi r_0^2(x)$ is the cross-section at rest with $r_0(x)$ being the corresponding radius. Applying the elastic law (1.3) to the 1-D blood flow system (1.1)–(1.2), we arrive at the following 1-D blood flow system in the form of hyperbolic balance laws:

$$A_t + Q_x = 0, \tag{1.4}$$

$$Q_t + \left(\frac{Q^2}{A} + \frac{\beta}{3} A^{\frac{3}{2}} \right)_x = \beta A \left(\sqrt{B} \right)_x - \alpha \frac{Q}{A}, \tag{1.5}$$

where $\beta = \kappa/\rho\sqrt{\pi}$.

The blood flow system (1.4)–(1.5) is similar to the 1-D shallow water equations, which has been widely used to model water flows in rivers, lakes, coastal areas as well as in a variety of oceanographic and atmospheric flows. As in the case of shallow water models, the main challenge in the development of robust and accurate numerical methods for the system (1.4)–(1.5) is to respect a delicate balance between the flux and the source terms in Eq. (1.5). Such methods are called WB. They are capable of exactly preserving discrete steady-state solutions

(equilibria) and accurately capturing nearly equilibrium flows even when a relatively coarse mesh is used.

It is easy to check that the system (1.4)–(1.5) admits a family of smooth steady states satisfying

$$Q(x) \equiv \widehat{Q} = \texttt{Const}, \quad \left[\frac{\widehat{Q}^2}{2A^2(x)} + \beta\left(\sqrt{A(x)} - \sqrt{B(x)}\right)\right]_x = -\alpha\frac{\widehat{Q}}{A^2(x)}. \quad (1.6)$$

There are several particular cases, which we will consider in the numerical examples in Sect. 3. In the frictionless case of $\alpha(x) \equiv 0$, (1.6) reduces to

$$Q(x) \equiv \widehat{Q}, \quad \frac{\widehat{Q}^2}{2A^2(x)} + \beta\left(\sqrt{A(x)} - \sqrt{B(x)}\right) \equiv \texttt{Const}. \quad (1.7)$$

If B is assumed to be constant, then $\left(\sqrt{B(x)}\right)_x \equiv 0$ and (1.6) can be simplified to

$$Q(x) \equiv \widehat{Q}, \quad -\widehat{Q}^2 \ln(A(x)) + \frac{\beta}{5} A^{\frac{5}{2}}(x) = -\alpha\widehat{Q}x + \texttt{Const}. \quad (1.8)$$

In the case of $Q \not\equiv 0$, the equilibria (1.6)–(1.8) correspond to the so-called "living-man" steady states, while in the motionless case, (1.6)–(1.8) reduce to the so-called "man-at-eternal-rest" or "dead-man" steady-states given by

$$Q(x) \equiv 0, \quad A(x) \equiv B(x). \quad (1.9)$$

Several WB numerical methods for the 1-D blood flow models have been recently proposed. In [8], first- and second-order finite-volume schemes capable of exactly preserving "dead-man" equilibria have been developed. In [20], a high-order weighted essentially non-oscillatory (WENO) scheme has been constructed for the 1-D blood flow in elastic vessels with varying mechanical and geometrical properties. In [2], a fully WB discontinuous Galerkin methods capable of exactly preserving both the "dead-man" and "living-man" equilibria have been derived by representing a solution in terms of the sum of the equilibrium and fluctuation following by rewriting the frictionless version of the system (1.4)–(1.5) in terms of the fluctuations (obviously, this method is based on the assumption that the background equilibrium state is a-priori known). In [10], a positivity preserving and fully WB scheme has been designed for the 1-D blood flow equations with friction, but with a constant cross-section at rest B. In [7], second-order WB Lagrange-projection schemes capable of exactly preserving "dead-man" equilibria have been developed for the frictionless 1-D blood flow system.

In this paper, we introduce a robust, highly accurate, semi-discrete, second-order central-upwind (CU) scheme for the 1-D blood flow model (1.4)–(1.5). CU schemes, originally developed in the context of general multidimensional hyperbolic systems of conservation laws in [14, 16, 18], belong to a class of Godunov-type Riemann-problem-solver-free finite-volume schemes and thus can be applied as a "black-box solver" to a wide variety of problems including several shallow water models; see, e.g., [13] and references therein. When CU schemes are applied to hyperbolic systems of balance laws, a robust way of preserving general steady-state solutions via flux globalization

was proposed in [5]: The source terms are first incorporated into the fluxes and then the CU scheme is applied to the resulting conservative system with global fluxes. This approach has been successfully applied to the Saint-Venant system of shallow water equations [3, 6], thermal rotating shallow water equations [15], and the compressible Euler equations with gravitation [4]. Here, we extend the flux globalization approach to the 1-D blood flow model and use it to develop the fully WB CU scheme for the system (1.4)–(1.5). In order to preserve the nonnegativity of the cross-sectional area A, we use the "draining time-step" technique originally introduced in [1] in the context of shallow water equations.

The rest of the paper is organized as follows. In Sect. 2, we introduce the flux globalization based WB CU scheme. First, in Sect. 2.1, we reformulate the studied blood flow system in an equivalent quasi-conservative form with a global flux. Then, in Sect. 2.2, we develop a WB CU scheme for the reformulated blood flow system. In Sect. 3, we present several numerical examples to demonstrate the performance of the proposed scheme.

2 Flux globalization based well-balanced scheme

In this section, we introduce the flux globalization based reformulation of the system (1.4)–(1.5) and then use it to develop the WB CU scheme.

2.1 Flux globalization

We first incorporate the source terms present on the right-hand side (RHS) of (1.5) into the fluxes and rewrite the system (1.4)–(1.5) in the following quasi-conservative form:

$$
\begin{aligned}
A_t + Q_x &= 0, \\
Q_t + K_x &= 0.
\end{aligned}
\tag{2.1}
$$

Here,

$$
K := \frac{Q^2}{A} + \frac{\beta}{3} A^{\frac{3}{2}} + R + S
\tag{2.2}
$$

is the global flux with the global variables:

$$
R(x, t) := -\beta \int_{\widehat{x}}^{x} A(\xi, t) \left(\sqrt{B(\xi, t)} \right)_x d\xi, \quad S(x, t) := \int_{\widehat{x}}^{x} \alpha(\xi) \frac{Q(\xi, t)}{A(\xi, t)} d\xi, \quad (2.3)
$$

where $\widehat{x}$ is an arbitrary number.

Smooth steady states of the system (2.1)–(2.3) can be written by

$$
Q(x) \equiv \widehat{Q} = \texttt{Const}, \quad K(x) \equiv \widehat{K} = \texttt{Const}.
\tag{2.4}
$$

Notice that (2.4) is equivalent to (1.6).

2.2 Well-balanced central-upwind scheme

We now develop a semi-discrete second-order WB CU scheme for the quasi-conservative system (2.1)–(2.3), which can be written in the vector form as

$$\boldsymbol{U}_t + \boldsymbol{F}(\boldsymbol{U})_x = \boldsymbol{0}, \tag{2.5}$$

where $\boldsymbol{U} = (A, Q)^\top$ and $\boldsymbol{F}(\boldsymbol{U}) = (Q, K)^\top$. In order to design the WB CU scheme for (2.5), we follow the lines of [3, 5, 6] and combine the Riemann-problem-solver-free CU evolution with the reconstruction of the equilibrium (flux) variables Q and K (rather than the conservative variables A and Q), which are constant at steady states.

To this end, we first introduce a uniform (for simplicity of presentation) finite-volume cells $C_j := [x_{j-\frac{1}{2}}, x_{j+\frac{1}{2}}]$ of size Δx centered at $x_j = (x_{j+\frac{1}{2}} + x_{j+\frac{1}{2}})/2$ and denote by $\overline{\boldsymbol{U}}_j(t)$ the cell average of $\boldsymbol{U}(\cdot, t)$ over C_j:

$$\overline{\boldsymbol{U}}_j(t) :\approx \frac{1}{\Delta x} \int_{C_j} \boldsymbol{U}(x, t) \, dx, \quad j = j_\ell, \dots, j_r.$$

We suppose that at certain time $t \geq 0$, the cell averages $\overline{\boldsymbol{U}}_j$ are available and from now on, we omit the time-dependence of all of the indexed quantities for the sake of brevity.

We then apply the semi-discrete CU scheme introduced in [14], according to which the cell averages of the solution are evolved in time by solving the following system of ODEs:

$$\frac{d}{dt} \overline{\boldsymbol{U}}_j = -\frac{\boldsymbol{H}_{j+\frac{1}{2}} - \boldsymbol{H}_{j-\frac{1}{2}}}{\Delta x}, \tag{2.6}$$

where the CU numerical flux is given by

$$\boldsymbol{H}_{j+\frac{1}{2}} = \frac{a^+_{j+\frac{1}{2}} \boldsymbol{F}^-_{j+\frac{1}{2}} - a^-_{j+\frac{1}{2}} \boldsymbol{F}^+_{j+\frac{1}{2}}}{a^+_{j+\frac{1}{2}} - a^-_{j+\frac{1}{2}}} + \frac{a^+_{j+\frac{1}{2}} a^-_{j+\frac{1}{2}}}{a^+_{j+\frac{1}{2}} - a^-_{j+\frac{1}{2}}} \left(\boldsymbol{U}^+_{j+\frac{1}{2}} - \boldsymbol{U}^-_{j+\frac{1}{2}} - \delta \boldsymbol{U}_{j+\frac{1}{2}} \right). \tag{2.7}$$

Here, $\boldsymbol{F}^\pm_{j+\frac{1}{2}}$ and $\boldsymbol{U}^\pm_{j+\frac{1}{2}}$ are reconstructed right/left-sided values of Q, K and A at the cell interface $x = x_{j+\frac{1}{2}}$, obtained using a special WB reconstruction procedure described in Sect. 2.2.1. The term $\delta \boldsymbol{U}_{j+\frac{1}{2}}$ represents a built-in "anti-diffusion" given by (see [14])

$$\delta \boldsymbol{U}_{j+\frac{1}{2}} = \text{minmod} \left(\boldsymbol{U}^+_{j+\frac{1}{2}} - \boldsymbol{U}^*_{j+\frac{1}{2}}, \; \boldsymbol{U}^*_{j+\frac{1}{2}} - \boldsymbol{U}^-_{j+\frac{1}{2}} \right), \tag{2.8}$$

where

$$U^*_{j+\frac{1}{2}} = \frac{a^+_{j+\frac{1}{2}} U^+_{j+\frac{1}{2}} - a^-_{j+\frac{1}{2}} U^-_{j+\frac{1}{2}} - \left\{ F(U^+_{j+\frac{1}{2}}) - F(U^-_{j+\frac{1}{2}}) \right\}}{a^+_{j+\frac{1}{2}} - a^-_{j+\frac{1}{2}}},$$

and the minmod function is defined by

$$\mathrm{minmod}(z_1, z_2, \ldots) := \begin{cases} \min_j \{z_j\} & \text{if } z_j > 0 \; \forall j, \\ \max_j \{z_j\} & \text{if } z_j < 0 \; \forall j, \\ 0 & \text{otherwise .} \end{cases}$$

Finally, $a^\pm_{j+\frac{1}{2}}$ are the one-sided local speeds of propagation, which can be estimated using the largest and the smallest eigenvalues of the Jacobian of the system (1.4)–(1.5) as follows:

$$a^+_{j+\frac{1}{2}} = \max \left\{ \frac{Q^+_{j+\frac{1}{2}}}{A^+_{j+\frac{1}{2}}} + \sqrt{\frac{\beta}{2}} (A^+_{j+\frac{1}{2}})^{\frac{1}{4}}, \frac{Q^-_{j+\frac{1}{2}}}{A^-_{j+\frac{1}{2}}} + \sqrt{\frac{\beta}{2}} (A^-_{j+\frac{1}{2}})^{\frac{1}{4}}, 0 \right\},$$

$$a^-_{j+\frac{1}{2}} = \min \left\{ \frac{Q^+_{j+\frac{1}{2}}}{A^+_{j+\frac{1}{2}}} - \sqrt{\frac{\beta}{2}} (A^+_{j+\frac{1}{2}})^{\frac{1}{4}}, \frac{Q^-_{j+\frac{1}{2}}}{A^-_{j+\frac{1}{2}}} - \sqrt{\frac{\beta}{2}} (A^-_{j+\frac{1}{2}})^{\frac{1}{4}}, 0 \right\}. \tag{2.9}$$

2.2.1 Well-balanced reconstruction

In order to complete the derivation of the WB CU scheme, we follow the lines of [6] to reconstruct the point values $Q^\pm_{j+\frac{1}{2}}$ and $K^\pm_{j+\frac{1}{2}}$, and then obtain the point values $A^\pm_{j+\frac{1}{2}}$.

We first follow the idea introduced in [17] in the context of WB CU scheme for the Saint-Venant system and replace the cross-section at rest function $B(x)$ with its continuous piecewise linear approximation:

$$\widetilde{B}(x) = B_{j-\frac{1}{2}} + \frac{B_{j+\frac{1}{2}} - B_{j-\frac{1}{2}}}{\Delta x} (x - x_{j-\frac{1}{2}}), \quad x \in C_j,$$

where

$$B_{j+\frac{1}{2}} := \frac{B(x_{j+\frac{1}{2}} + 0) + B(x_{j+\frac{1}{2}} - 0)}{2},$$

which reduces to $B_{j+\frac{1}{2}} := B(x_{j+\frac{1}{2}})$ if B is continuous at $x = x_{j+\frac{1}{2}}$. We then introduce the following notations:

$$B_j := \widetilde{B}(x_j) = \frac{B_{j+\frac{1}{2}} + B_{j-\frac{1}{2}}}{2}, \quad (B_x)_j := \widetilde{B}_x(x_j) = \frac{B_{j+\frac{1}{2}} - B_{j-\frac{1}{2}}}{\Delta x}.$$

In order to evaluate the global variables R and S, we begin with computing their point values by discretizing the integrals in (2.3). First, we set $\hat{x} = x_{j_\ell - \frac{1}{2}}$ so that

$$R_{j_\ell - \frac{1}{2}} := 0, \quad S_{j_\ell - \frac{1}{2}} := 0, \tag{2.10}$$

and then use midpoint-type quadratures to obtain following recursive formulae for the values of R and S at the cell interfaces $x = x_{j+\frac{1}{2}}$:

$$R_{j+\frac{1}{2}} = R_{j-\frac{1}{2}} - \beta \overline{A}_j\left(\sqrt{B_{j+\frac{1}{2}}} - \sqrt{B_{j-\frac{1}{2}}}\right),$$
$$S_{j+\frac{1}{2}} = S_{j-\frac{1}{2}} + \Delta x\, \alpha(x_j)\frac{\overline{Q}_j}{\overline{A}_j}, \qquad j = j_\ell, \dots, j_r.$$

Next, we approximate the values of R and S at the cell centers $x = x_j$. To this end, we first write the recursive formulae

$$R_{j+1} = R_j - \beta \int_{x_j}^{x_{j+1}} A(\sqrt{B})_x \, \mathrm{d}x, \quad S_{j+1} = S_j + \int_{x_j}^{x_{j+1}} \alpha\frac{Q}{A} \, \mathrm{d}x, \tag{2.11}$$

and then derive a special quadrature for the first integral in (2.11). This quadrature will be WB in the sense that in the case the data correspond to the "dead-man" equilibrium (1.9), all of the values K_j should be the same (in particular, $K_j = K_{j+1}$). Thus, using the definition of K in (2.2), (2.3), we would require that at the steady state (1.9)

$$\frac{\beta}{3}(\overline{A}_{j+1})^{\frac{3}{2}} - \beta \int_{x_j}^{x_{j+1}} A(\sqrt{B})_x \, \mathrm{d}x = \frac{\beta}{3}(\overline{A}_j)^{\frac{3}{2}}. \tag{2.12}$$

The WB quadrature is then

$$\int_{x_j}^{x_{j+1}} A(\sqrt{B})_x \, \mathrm{d}x \approx \frac{1}{3}\left(\overline{A}_j + \overline{A}_{j+1} + \sqrt{\overline{A}_j \overline{A}_{j+1}}\right)\left(\sqrt{B_{j+1}} - \sqrt{B_j}\right). \tag{2.13}$$

Indeed, when at the steady state $\overline{A}_j = B_j$ and $\overline{A}_{j+1} = B_{j+1}$, the RHS of (2.13) reduces to

$$\frac{1}{3}\left(B_j + B_{j+1} + \sqrt{B_j B_{j+1}}\right)\left(\sqrt{B_{j+1}} - \sqrt{B_j}\right) = \frac{1}{3}\left[(B_{j+1})^{\frac{3}{2}} - (B_j)^{\frac{3}{2}}\right] \tag{2.14}$$

and then substituting $\overline{A}_j = B_j$, $\overline{A}_{j+1} = B_{j+1}$, (2.13) and (2.14) into (2.12) results in an identity.

The second integral in (2.11) is discretized using the trapezoidal rule and the resulting recursive formulae for the values of R and S at the cell centers are

$$R_{j+1} = R_j - \frac{\beta}{3}\left(\overline{A}_j + \overline{A}_{j+1} + \sqrt{\overline{A}_j \overline{A}_{j+1}}\right)\left(\sqrt{B_{j+1}} - \sqrt{B_j}\right), \quad j = j_\ell, \dots, j_r - 1,$$

(2.15)

$$S_{j+1} = S_j + \frac{\Delta x}{2}\left(\alpha(x_j)\frac{\overline{Q}_j}{\overline{A}_j} + \alpha(x_{j+1})\frac{\overline{Q}_{j+1}}{\overline{A}_{j+1}}\right), \quad j = j_\ell, \dots, j_r - 1.$$

(2.16)

The first two terms in (2.15) and (2.16), namely, R_{j_ℓ} and S_{j_ℓ}, are computed using the similar quadratures and by taking into account (2.10):

$$R_{j_\ell} = -\frac{\beta}{3}\left(A_{j_\ell - \frac{1}{2}} + \overline{A}_{j_\ell} + \sqrt{A_{j_\ell - \frac{1}{2}}\overline{A}_{j_\ell}}\right)\left(\sqrt{B_{j_\ell}} - \sqrt{B_{j_\ell - \frac{1}{2}}}\right),$$

(2.17)

$$S_{j_\ell} = \frac{\Delta x}{4}\left(\alpha(x_{j_\ell})\frac{\overline{Q}_{j_\ell}}{\overline{A}_{j_\ell}} + \alpha(x_{j_\ell - \frac{1}{2}})\frac{Q^+_{j_\ell - \frac{1}{2}}}{A_{j_\ell - \frac{1}{2}}}\right),$$

(2.18)

where $Q^+_{j_\ell - \frac{1}{2}}$ is a reconstructed point value of Q, obtained using a piecewise linear reconstruction described below (see (2.20)–(2.21)), and $A_{j_\ell - \frac{1}{2}}$ is computed by numerically solving the following nonlinear equation:

$$\frac{\left(Q^+_{j_\ell - \frac{1}{2}}\right)^2}{A_{j_\ell - \frac{1}{2}}} + \frac{\beta}{3}\left(A_{j_\ell - \frac{1}{2}}\right)^{\frac{3}{2}} = \frac{\left(\overline{Q}_{j_\ell}\right)^2}{\overline{A}_{j_\ell}} + \frac{\beta}{3}\left(\overline{A}_{j_\ell}\right)^{\frac{3}{2}} + R_{j_\ell} + S_{j_\ell},$$

which corresponds to the boundary condition $K_{j_\ell - \frac{1}{2}} = K_{j_\ell}$, which should be used if the solution is at steady state at the boundary.

Remark 2.1 Depending on a problem at hand, an alternative boundary condition for $A_{j_\ell - \frac{1}{2}}$ can be used.

Equipped with the point values R_j and S_j, we use (2.2) to obtain

$$K_j = \frac{\left(\overline{Q}_j\right)^2}{\overline{A}_j} + \frac{\beta}{3}\left(\overline{A}_j\right)^{\frac{3}{2}} + R_j + S_j,$$

introduce the equilibrium (flux) variables $\boldsymbol{F}_j := \left(\overline{Q}_j, K_j\right)^\top$, and then perform a piecewise linear reconstruction

$$\widetilde{\boldsymbol{F}}(x) = \boldsymbol{F}_j + (\boldsymbol{F}_x)_j(x - x_j), \quad x \in C_j,$$

(2.19)

which is used to evaluate the right/left-sided values $F^{\pm}_{j+\frac{1}{2}}$ at the cell interface $x = x_{j+\frac{1}{2}}$:

$$F^-_{j+\frac{1}{2}} = F_j + \frac{\Delta x}{2}(F_x)_j, \quad F^+_{j+\frac{1}{2}} = F_{j+1} - \frac{\Delta x}{2}(F_x)_{j+1}. \tag{2.20}$$

In order to ensure a non-oscillatory nature of the piecewise linear reconstruction (2.19) and the resulting scheme, one needs to compute the slopes $(F_x)_j$ with the help of a nonlinear limiter. In all of the numerical experiments reported in Sect. 3, we have used a generalized minmod limiter [19, 21, 23]:

$$(F_x)_j = \text{minmod}\left(\theta\,\frac{F_j - F_{j-1}}{\Delta x},\; \frac{F_{j+1} - F_{j-1}}{2\Delta x},\; \theta\,\frac{F_{j+1} - F_j}{\Delta x}\right), \quad \theta \in [1, 2], \tag{2.21}$$

applied in the component-wise manner. The parameter θ in (2.21) can be used to control the oscillations in the computed solution as larger θ's correspond to less dissipative but, in general, more oscillatory reconstructions.

Finally, after $F^{\pm}_{j+\frac{1}{2}} = \left(Q^{\pm}_{j+\frac{1}{2}}, K^{\pm}_{j+\frac{1}{2}}\right)^{\top}$ have been computed, we obtain $A^{\pm}_{j+\frac{1}{2}}$ by numerically solving the following nonlinear equations:

$$K^i_{j+\frac{1}{2}} = \frac{\left(Q^i_{j+\frac{1}{2}}\right)^2}{A^i_{j+\frac{1}{2}}} + \frac{\beta}{3}\left(A^i_{j+\frac{1}{2}}\right)^{\frac{3}{2}} + R_{j+\frac{1}{2}} + S_{j+\frac{1}{2}}, \quad i \in \{+, -\}. \tag{2.22}$$

In the numerical experiments reported in Sect. 3, these equations are solved using Newton's method; see Appendix A for details.

Remark 2.2 We emphasize that if the discrete data correspond to the steady state, that is, if $\overline{Q}_j \equiv \widehat{Q}$, $K_j \equiv \widehat{K}$, $\forall j$, then $Q^+_{j+\frac{1}{2}} = Q^-_{j+\frac{1}{2}} \equiv \widehat{Q}$, $K^+_{j+\frac{1}{2}} = K^-_{j+\frac{1}{2}} \equiv \widehat{K}$, $\forall j$, which implies that the equations for $i = +$ and $i = -$ in (2.22) are identical, which ensures that $A^+_{j+\frac{1}{2}} = A^-_{j+\frac{1}{2}}$, $\forall j$ and therefore the numerical fluxes (2.7) would be $H_{j+\frac{1}{2}} \equiv (\widehat{Q}, \widehat{K})^{\top}$, $\forall j$ and hence the RHS of (2.6) would vanish. This proves that the developed flux globalization based CU scheme is WB in the sense that it is capable of exactly preserving discrete steady states

$$\overline{Q}_j \equiv \widehat{Q}, \quad K_j \equiv \widehat{K}, \; \forall j. \tag{2.23}$$

Remark 2.3 The nonnegativity of the computed cell averages $\overline{A}_j$ is enforced using the "draining time-step" technique originally introduced in [1] in the context of shallow water equations.

3 Numerical examples

In this section, we first test the proposed flux globalization based WB CU scheme on several benchmarks from [10] and [2], where the systems

$$
\text{Model I :} \quad
\begin{cases}
A_t + Q_x = 0, \\
Q_t + \left(\dfrac{Q^2}{A} + \dfrac{\beta}{3} A^{\frac{3}{2}} \right)_x = -\alpha \dfrac{Q}{A},
\end{cases}
$$

and

$$
\text{Model II :} \quad
\begin{cases}
A_t + Q_x = 0, \\
Q_t + \left(\dfrac{Q^2}{A} + \dfrac{\beta}{3} A^{\frac{3}{2}} \right)_x = \beta A \left(\sqrt{B} \right)_x,
\end{cases}
$$

respectively, have been studied. We note that Model I is the system (1.4)–(1.5) with the constant cross-section at rest, that is, with $B(x) \equiv \texttt{Const}$, while Model II is a frictionless (with $\alpha = 0$) version of the system (1.4)–(1.5).

We then test the performance of the flux globalization based WB CU on an example for the general system (1.4)–(1.5). The obtained results are compared with those computed by the non-well-balanced (NWB) CU scheme described in Appendix B. For the sake of brevity, the two studied schemes will be referred to as the WB and NWB schemes in all of the examples below. In all of the numerical examples, we use the WB scheme on a very fine mesh with 20,000 uniform cells to compute reference solutions. For the sake of brevity, the solutions computed by the WB and NWB schemes on a coarse mesh with 200 uniform cells will be referred to as the WB solution and NWB solution, respectively.

In all of the examples, the time evolution is carried out using the three-stage third-order strong stability preserving (SSP) Runge–Kutta method (see, e.g., [11, 12]) with the CFL number 0.5. The minmod parameter has been set to $\theta = 1.3$.

3.1 Numerical tests for model I

In this section, we apply the studied WB and NWB CU schemes to Model I with $\beta = 176\sqrt{\pi} \times 10^5 / 9891$ and test them on three numerical examples taken from [10, § 6.3].

For Model I, the "living-man" steady state (1.8) can be written as

$$
Q(x) \equiv \widehat{Q}, \quad -\widehat{Q}^2 \ln(A(x)) + \frac{\beta}{5} A^{\frac{5}{2}}(x) = -\alpha \widehat{Q}(x - x_{\text{ref}}) \\
- \widehat{Q}^2 \ln(A_{\text{ref}}) + \frac{\beta}{5} A_{\text{ref}}^{\frac{5}{2}}, \tag{3.1}
$$

where A_{ref} is a reference value of $A(x)$ at a certain reference point $x = x_{\text{ref}}$ (in Example 1–3, $x_{\text{ref}} = 0$ and $A_{\text{ref}} = 3.14 \times 10^{-4}$).

In order to express the discrete version of the steady state (3.1) in terms of the global flux K, that is, using (2.4), we substitute $x = x_{j_\ell - \frac{1}{2}}$ into (3.1) and solve the resulting nonlinear equation

$$-\widehat{Q}^2 \ln\left(A_{j_\ell - \frac{1}{2}}\right) + \frac{\beta}{5} A_{j_\ell - \frac{1}{2}}^{\frac{5}{2}} = -\alpha\widehat{Q}(x_{j_\ell - \frac{1}{2}} - x_{\mathrm{ref}}) - \widehat{Q}^2 \ln(A_{\mathrm{ref}}) + \frac{\beta}{5} A_{\mathrm{ref}}^{\frac{5}{2}}.$$

for $A_{j_\ell - \frac{1}{2}}$. We then use (2.2) and (2.10) to obtain

$$K_{j_\ell - \frac{1}{2}} = \frac{\widehat{Q}^2}{A_{j_\ell - \frac{1}{2}}} + \frac{\beta}{3} A_{j_\ell - \frac{1}{2}}^{\frac{3}{2}} = \widehat{K}, \tag{3.2}$$

and then we have $K_j \equiv \widehat{K}$, $\forall j$. Finally, the values $\overline{A}_j$ are recursively obtained from (2.23) as follows. First, we use (2.2) with $R = 0$, (2.23) and (2.18) to construct the nonlinear equation for $\overline{A}_{j_\ell}$:

$$\frac{\widehat{Q}^2}{\overline{A}_{j_\ell}} + \frac{\beta}{3} \overline{A}_{j_\ell}^{\frac{3}{2}} + \frac{\widehat{Q}\Delta x}{4}\left[\frac{\alpha(x_{j_\ell})}{\overline{A}_{j_\ell}} + \frac{\alpha(x_{j_\ell - \frac{1}{2}})}{A_{j_\ell - \frac{1}{2}}}\right] = \widehat{K}, \tag{3.3}$$

and after solving (3.3), we proceed with solving the following sequence of nonlinear equations:

$$\frac{\widehat{Q}^2}{\overline{A}_{j+1}} + \frac{\beta}{3} \overline{A}_{j+1}^{\frac{3}{2}} + S_j + \frac{\widehat{Q}\Delta x}{2}\left[\frac{\alpha(x_{j+1})}{\overline{A}_{j+1}} + \frac{\alpha(x_j)}{\overline{A}_j}\right] = \widehat{K}, \quad j = j_\ell, \ldots, j_r - 1, \tag{3.4}$$

where the global variable S_j is obtained using Eq. (2.16). Finally, Eq. (3.4) are to be solved recursively for $\overline{A}_{j+1}$. Both (3.3) and (3.4) are numerically solver using Newton's method with A_{ref} being used as an initial guess.

In Examples 1–3 studied in this section, we prescribe the Dirichlet boundary conditions, namely, the values of $\boldsymbol{F}$ at the left and right endpoints of the computational domain. We first set the point values $\boldsymbol{F}_{j_\ell - \frac{1}{2}}^-$ and $\boldsymbol{F}_{j_r + \frac{1}{2}}^+$ to equal to the corresponding prescribed boundary values, and after that we use these values to compute the slopes $(\boldsymbol{F})_x$ in the cells C_{j_ℓ} and C_{j_r}, where one cannot use formula (2.21), as follows:

$$(\boldsymbol{F}_x)_{j_\ell} = \mathrm{minmod}\left(\frac{\boldsymbol{F}_{j_\ell} - \boldsymbol{F}_{j_\ell - \frac{1}{2}}^-}{\Delta x/2}, \frac{\boldsymbol{F}_{j_\ell + 1} - \boldsymbol{F}_{j_\ell}}{\Delta x}\right), \tag{3.5}$$

$$(\boldsymbol{F}_x)_{j_r} = \mathrm{minmod}\left(\frac{\boldsymbol{F}_{j_r} - \boldsymbol{F}_{j_r - 1}}{\Delta x}, \frac{\boldsymbol{F}_{j_r + \frac{1}{2}}^+ - \boldsymbol{F}_{j_r}}{\Delta x/2}\right). \tag{3.6}$$

We then use these slopes to compute the point values in cells C_{j_ℓ} and C_{j_r}:

$$\boldsymbol{F}_{j_\ell - \frac{1}{2}}^+ = \overline{\boldsymbol{F}}_{j_\ell} - \frac{\Delta x}{2}(\boldsymbol{F}_x)_{j_\ell}, \quad \boldsymbol{F}_{j_\ell + \frac{1}{2}}^- = \overline{\boldsymbol{F}}_{j_\ell} + \frac{\Delta x}{2}(\boldsymbol{F}_x)_{j_\ell}, \tag{3.7}$$

$$F^+_{j_r - \frac{1}{2}} = \overline{F}_{j_r} - \frac{\Delta x}{2}(F_x)_{j_r}, \quad F^-_{j_r + \frac{1}{2}} = \overline{F}_{j_r} + \frac{\Delta x}{2}(F_x)_{j_r}. \tag{3.8}$$

Finally, the boundary point values $A^-_{j_\ell - \frac{1}{2}}$ and $A^+_{j_r + \frac{1}{2}}$ are calculated by solving the non-linear equation (2.22).

3.1.1 Example 1—WB assessment with constant α

In the first example, we demonstrate that the proposed flux globalization based WB CU scheme is capable of exactly preserving "living-man" steady state taken from [10] and accurately handling their small perturbations.

We take a constant viscous resistance $\alpha(x) \equiv 11\pi/210{,}000$ (m^2/s^2) and begin with the initial data corresponding to the discrete equilibrium: $\overline{Q}^{\mathrm{E}}_j \equiv \widehat{Q} = -10^{-3}$ m^3/s and $K^{\mathrm{E}}_j \equiv \widehat{K}$ with the value $\widehat{K}$ as well as the cell averages of A, namely, $\overline{A}^{\mathrm{E}}_j$ obtained using (3.1)–(3.4). We compute the numerical solutions until the final time $t = 5$ s using both the WB and NWB schemes with 200 uniform cells on the computational domain $[-\pi/2, \pi/2]$ with the Dirichlet boundary conditions.

We first compute the L^1- and L^2-errors denoted by $e_1(t)$ and $e_2(t)$ and defined as follows:

$$e_1(t) := \Delta x \sum_{j=j_\ell}^{j_r} |\overline{A}_j(t) - \overline{A}^{\mathrm{E}}_j| + \Delta x \sum_{j=j_\ell}^{j_r} |\overline{Q}_j(t) - \overline{Q}^{\mathrm{E}}_j|,$$
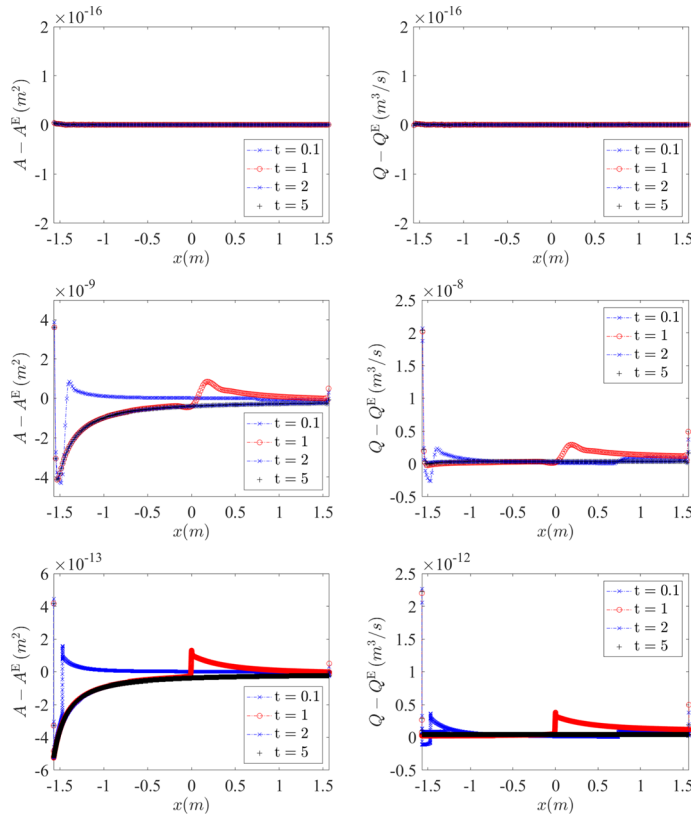
$$e_2(t) := \left[\Delta x \sum_{j=j_\ell}^{j_r} \left(\overline{A}_j(t) - \overline{A}^{\mathrm{E}}_j \right)^2 + \Delta x \sum_{j=j_\ell}^{j_r} \left(\overline{Q}_j(t) - \overline{Q}^{\mathrm{E}}_j \right)^2 \right]^{\frac{1}{2}},$$

at times $t = 0.1, 1, 2$, and 5 s. The obtained results are presented in Table 1, where one can clearly see that unlike the NWB scheme, the proposed flux globalization based WB CU scheme preserves the steady state within the machine accuracy. In addition, in Fig. 1, we present the differences between the steady state and the solutions computed by the WB and NWB schemes (for the latter one we also show the solution computed on a substantially refined mesh with 20,000 uniform cells). As one can see, the error in the NWB scheme roughly reduces by a factor of 10^4, which confirms that the NWB scheme is indeed second-order accurate, but the error is still larger than the machine accuracy despite using so fine mesh.

We then slightly perturb the studied steady state by replacing the cell averages $\overline{A}_j(0) = \overline{A}^{\mathrm{E}}_j$ for $x_j \in [-\pi/20, \pi/20]$ with $\overline{A}_j(0) = \overline{A}^{\mathrm{E}}_j \left(1 - \epsilon \cos(10 x_j) \right)^2$ with

Table 1 Example 1: L^1- and L^2-errors for the WB and NWB schemes

|	$e_1(0.1)$	$e_1(1)$	$e_1(2)$	$e_1(5)$	$e_2(0.1)$	$e_2(1)$	$e_2(2)$	$e_2(5)$
WB	8.05e−19	8.05e−19	8.05e−19	8.05e−19	9.98e−19	9.98e−19	9.98e−19	9.98e−19
NWB	2.94e−9	5.40e−9	3.84e−9	3.78e−9	3.09e−9	3.87e−9	3.29e−9	3.26e−9
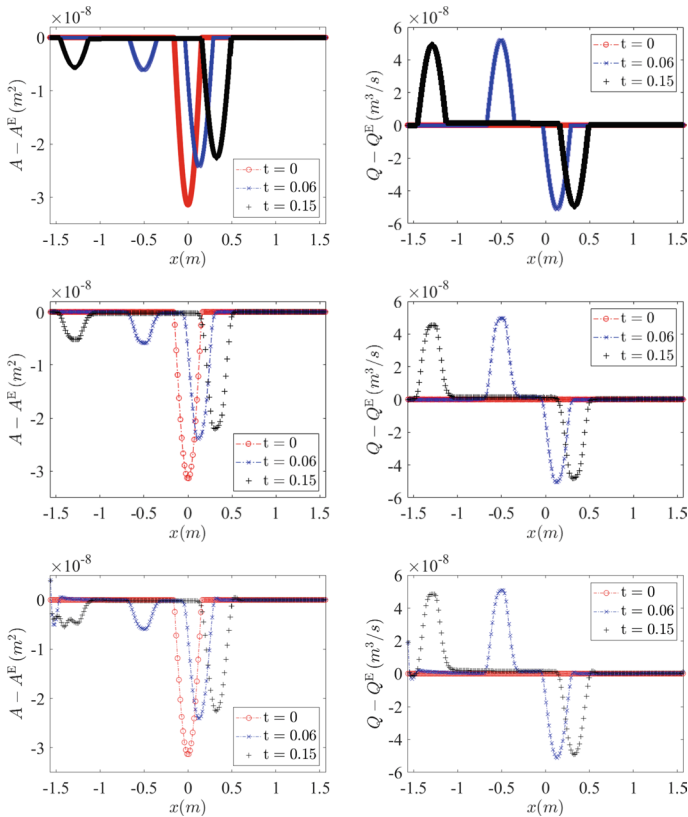
Fig. 1 Example 1: Differences between the steady states and solutions computed by the WB scheme on 200 uniform cells (top row) and the NWB scheme on 200 (middle row) and 20,000 (bottom row) uniform cells at four different times

$\varepsilon = 5 \times 10^{-5}$. We compute the numerical solutions by both the WB and NWB schemes until the final time $t = 0.15$ and present the obtained differences between the perturbed solutions and the steady state in Fig. 2. One can see that while the WB scheme captures the small perturbation in a non-oscillatory manner, the NWB scheme develops relatively large oscillations near the left end of the computational domain. Even though these oscillations decay when the mesh is refined, the obtained results clearly demonstrate the superiority of the WB scheme over the NWB one.

3.1.2 Example 2—WB assessment with nonconstant α

In the second example taken from [10], we choose the nonconstant viscous resistance

$$\alpha(x) = \frac{11\pi}{210{,}000}\left[1 + 0.1\sin\left(\frac{4\pi}{3}x\right)\right].$$
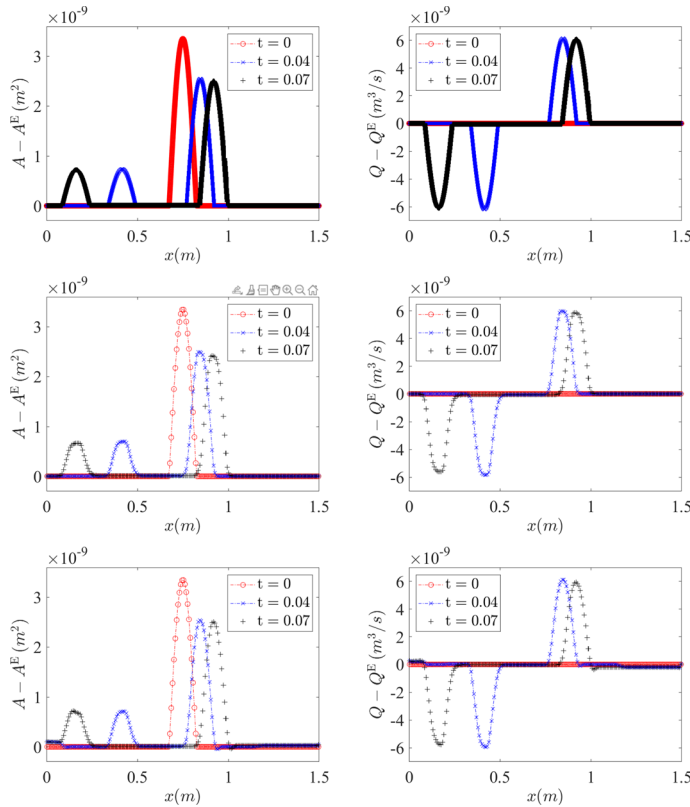
Fig. 2 Example 1: Differences between the reference (top row), WB (middle row), and NWB (bottom row) solutions and the steady state at three different times

As in Example 1, we consider the steady state solution with $\overline{Q}_j^{\mathrm{E}} \equiv \widehat{Q} = -10^{-3}$ m^3/s and $K_j^{\mathrm{E}} \equiv \widehat{K}$ with the value $\widehat{K}$ as well as the cell averages $\overline{A}_j^{\mathrm{E}}$ obtained using (3.1)–(3.4). The initial data given by

$$\overline{A}_j(0) = \begin{cases} \overline{A}_j^{\mathrm{E}}\left[1 - \varepsilon \cos\left(\frac{20\pi}{3}x_j\right)\right]^2 & \text{if } x \in \left[\frac{27}{40}, \frac{33}{40}\right], \\ \overline{A}_j^{\mathrm{E}} & \text{otherwise}, \end{cases} \qquad \overline{Q}_j(0) \equiv \widehat{Q},$$

contain a perturbation of A, which is small as we take $\varepsilon = 5 \times 10^{-6}$.

We compute the numerical solutions by both the WB and NWB schemes until the final time $t = 0.07$ s in the computational domain $[0, 1.5]$. The differences between the perturbed solutions and the steady state are presented in Fig. 3. As one can see, the WB scheme captures the small perturbation in a non-oscillatory way, while the NWB scheme develops some small oscillations near $x = 1$ and is also not very accurate at the left edge of the computational domain.

Fig. 3 Example 2: Differences between the reference (top row), WB (middle row), and NWB (bottom row) solutions and the steady state at three different times

3.1.3 Example 3—WB assessment with unknown α

In the third example taken from [10], we consider the case where the viscous resistance $\alpha(x)$ is initially unknown and computed as follows. For the data $A = A^{E}(x)$, $Q = Q^{E}(x) \equiv \widehat{Q}$ being at a steady state, the viscous resistance $\alpha(x)$ is obtained from the second equation of Model I and it is

$$\alpha(x) = -\frac{A^{E}(x)}{\widehat{Q}}\left(\frac{\widehat{Q}^{2}}{A^{E}(x)} + \frac{\beta}{3}\left(A^{E}(x)\right)^{\frac{3}{2}}\right)_{x} = \left(\frac{\widehat{Q}}{A^{E}(x)} - \frac{\beta\left(A^{E}(x)\right)^{\frac{3}{2}}}{2\widehat{Q}}\right)A^{E}_{x}(x).$$

$$(3.9)$$

In this example, we take the following continuous steady state:
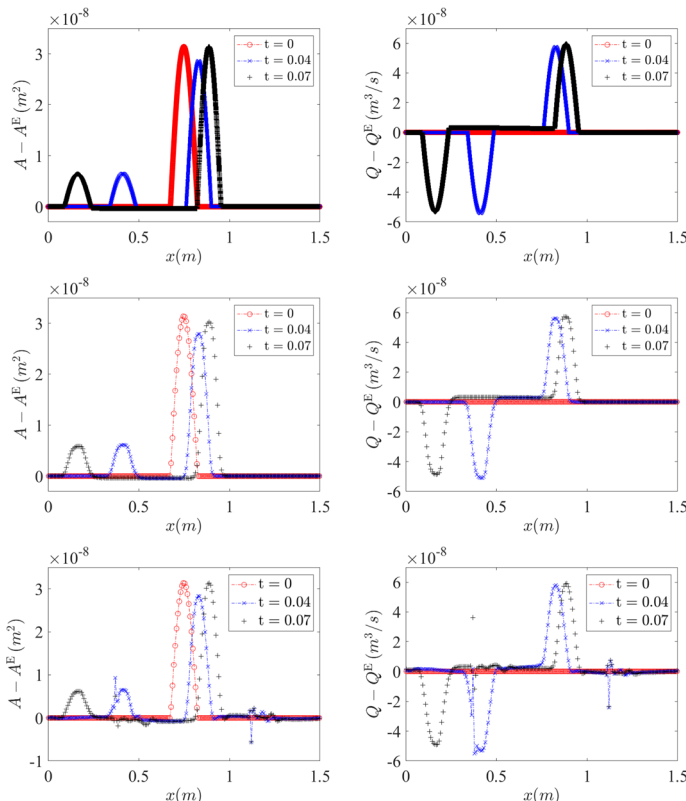
$$A^{E}(x) = \mathcal{A}\left[1 + 0.1\sin\left(\frac{4\pi}{3}x\right)\right], \quad Q^{E}(x) \equiv \widehat{Q} = -10^{-3} \text{ m}^{3}/s,$$

where $\mathcal{A} = 3.14 \times 10^{-4}$ m^2. We then compute the viscous resistance $\alpha(x)$ from (3.9), and the discrete steady state values $\overline{A}_j^{\mathrm{E}}$ and $K_j^{\mathrm{E}} \equiv \widehat{K}$ are obtained using (3.1)–(3.4). We take the initial data

$$\overline{A}_j(0) = \begin{cases} \overline{A}_j^{\mathrm{E}}\left[1 - \varepsilon \cos\left(\dfrac{20\pi}{3} x_j\right)\right]^2 & \text{if } x \in \left[\dfrac{27}{40}, \dfrac{33}{40}\right], \\ \overline{A}_j^{\mathrm{E}} & \text{otherwise}, \end{cases} \qquad \overline{Q}_j(0) \equiv -10^{-3},$$

which contain a small perturbation of A^{E} as $\varepsilon = 5 \times 10^{-5}$.

We compute the numerical solution by both the WB and NWB schemes until the final time $t = 0.07$ s in the computational domain [0, 1.5]. The differences between the perturbed solutions and the steady state are presented in Fig. 4. As one can see, the WB scheme still captures the perturbation very accurately, while the NWB scheme produces spurious oscillations throughout the entire computational domain.

Fig. 4 Example 3: Differences between the reference (top row), WB (middle row), and NWB (bottom row) solutions and the steady state at three different times

3.2 Numerical tests for Model II

In this section, we apply the studied WB and NWB CU scheme to Model II with $\beta = 5 \times 10^6 / 53\sqrt{\pi}$ and present three numerical experiments.

Recall that the steady states for Model II are given by

$$Q(x) \equiv \hat{Q}, \quad \frac{\hat{Q}^2}{2A^2(x)} + \beta\left(\sqrt{A(x)} - \sqrt{B(x)}\right) \equiv \hat{E}, \tag{3.10}$$

where $\hat{Q}$ and $\hat{E}$ are constants; see (1.7). In order to express the discrete version of (3.10) in terms of the global flux K, we first compute $A_{j_\ell - \frac{1}{2}}$ by solving the following nonlinear equation:

$$\frac{\hat{Q}^2}{2A^2_{j_\ell - \frac{1}{2}}} + \beta\left(\sqrt{A_{j_\ell - \frac{1}{2}}} - \sqrt{B_{j_\ell - \frac{1}{2}}}\right) = \hat{E}. \tag{3.11}$$

Equipped with $A_{j_\ell - \frac{1}{2}}$, we compute the constant $\hat{K}$ using (3.2) and then the cell-averages $\overline{A}_j$ can be computed recursively as follows. First, we construct the nonlinear equation for $\overline{A}_{j_\ell}$ using (2.2) with $S = 0$, (2.23) and (2.17):

$$\frac{\hat{Q}^2}{\overline{A}_{j_\ell}} + \frac{\beta}{3}(\overline{A}_{j_\ell})^{\frac{3}{2}} - \frac{\beta}{3}\left(A_{j_\ell - \frac{1}{2}} + \overline{A}_{j_\ell} + \sqrt{A_{j_\ell - \frac{1}{2}}\overline{A}_{j_\ell}}\right)\left(\sqrt{B_{j_\ell}} - \sqrt{B_{j_\ell - \frac{1}{2}}}\right) = \hat{K}. \tag{3.12}$$

After obtaining $\overline{A}_{j_\ell}$ from (3.12), the values of $\overline{A}_j$ can be computed by solving the following sequence of nonlinear equations:

$$\frac{\hat{Q}^2}{\overline{A}_{j+1}} + \frac{\beta}{3}\overline{A}_{j+1}^{\frac{3}{2}} + R_j - \frac{\beta}{3}\left(\overline{A}_j + \overline{A}_{j+1} + \sqrt{\overline{A}_j \overline{A}_{j+1}}\right)\left(\sqrt{B_{j+1}} - \sqrt{B_j}\right)$$
$$= \hat{K}, \quad j = j_\ell, \ldots, j_r - 1, \tag{3.13}$$

for $\overline{A}_{j+1}$. In (3.13), R_j is obtained using Eq. (2.15).

In this section, the computational domain is $[0, L]$ and the values of $\hat{Q}$ and $\hat{E}$ are defined as in [2, §5.2]:

$$\hat{Q} = Q_{\text{in}}, \quad \hat{E} = \frac{Q_{\text{in}}^2}{2A_{\text{out}}^2} + \beta\left(\sqrt{A_{\text{out}}} - \sqrt{B(L)}\right), \tag{3.14}$$

where the subscripts "in" and "out" represent the values at the inlet (left endpoint) and the outlet (right endpoint) of the domain. The values of Q_{in} and A_{out} in (3.14) are defined by

$$Q_{\text{in}} = A_{\text{in}} S_{\text{in}} C_{\text{in}}, \quad A_{\text{out}} = B(L)(1 + S_{\text{in}})^2, \quad A_{\text{in}} = B(0)(1 + S_{\text{in}})^2, \tag{3.15}$$

where S_{in} is the Shapiro number and $C_{in} = \sqrt{\beta\sqrt{A_{in}}}/2$ is the Moens–Korteweg velocity at the inlet. The nonlinear equations in (3.11) and (3.13) are solved using Newton's method with A_{in} being used as an initial guess.

3.2.1 Example 4—Perturbation of a "Dead Man" WB problem

In this example taken from [2, §3.3.3], we consider the case of "a dead man" with stenosis. The stenosis occurs when the artery becomes narrow and it will reduce the blood flow from the heart to the rest of the body. Here,

$$B(x) = \pi r_0^2(x), \quad \widehat{Q} = \widehat{E} = 0,$$

where $r_0(x)$ is the radius of artery at rest defined by

$$r_0(x) = \begin{cases} \tilde{r} + \Delta r, & x \in [0, x_1] \cup [x_4, L], \\ \tilde{r} + \frac{\Delta r}{2}\left[\cos\left(\frac{x-x_1}{x_2-x_1}\pi\right) + 1\right], & x \in [x_1, x_2], \\ \tilde{r}, & x \in [x_2, x_3], \\ \tilde{r} - \frac{\Delta r}{2}\left[\cos\left(\frac{x-x_3}{x_4-x_3}\pi\right) - 1\right], & x \in [x_3, x_4]. \end{cases}$$

Here, $\tilde{r} = 0.1$ m, $\Delta r = 10^{-3}$ m, $L = 0.14$ m, $x_1 = 9L/40$, $x_2 = L/4$, $x_3 = 3L/4$, and $x_4 = 33L/40$.
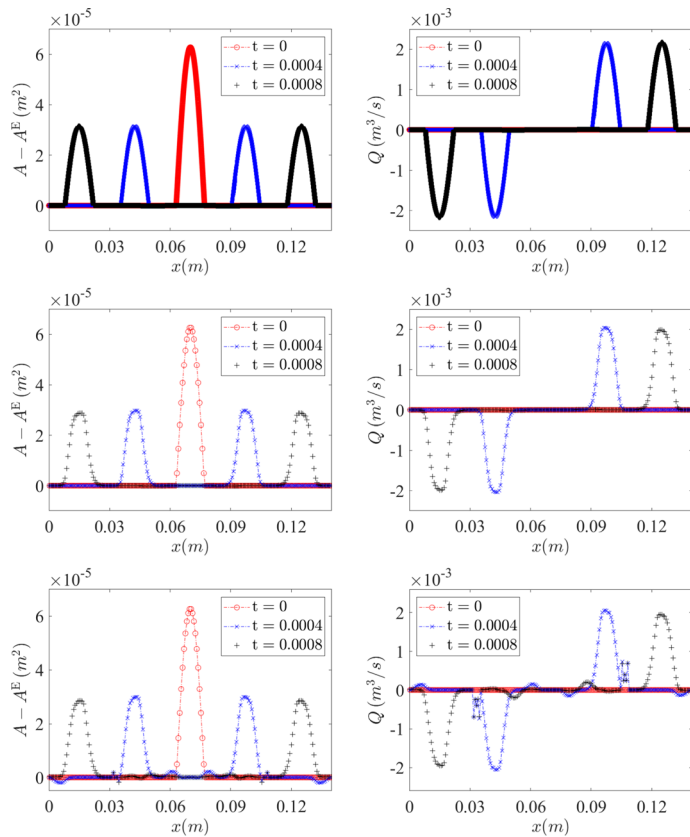
We first compute the discrete steady state solution with $\overline{Q}_j^E \equiv \widehat{Q} = 0$ and $K_j^E \equiv \widehat{K}$ with the value $\widehat{K}$ as well as the cell averages $\overline{A}_j^E$ obtained using (3.10)–(3.13), and then take the initial data

$$\overline{A}_j(0) = \begin{cases} \overline{A}_j^E\left[1 - \varepsilon\cos\left(\frac{500\pi}{7}x_j\right)\right]^2 & \text{if} \in \left[\frac{9L}{20}, \frac{11L}{20}\right], \\ \overline{A}_j^E & \text{otherwise}, \end{cases} \qquad \overline{Q}_j(0) \equiv 0,$$

which contains a small perturbation of A^E as we take $\varepsilon = 10^{-3}$ or $\varepsilon = 10^{-4}$. We use free boundary conditions at both $x = 0$ and $x = L$.

We compute the solutions by both the WB and NWB schemes until the final time $t = 0.0008$ s. The differences between the perturbed solutions and the steady state are presented in Figs. 5 and 6, where one can clearly see that the WB scheme can capture the perturbation accurately and in a non-oscillatory manner for both $\varepsilon = 10^{-3}$ and $\varepsilon = 10^{-4}$. On the contrary, the NWB scheme develops substantial oscillations for $\varepsilon = 10^{-3}$; see Fig. 5. For the smaller $\varepsilon = 10^{-4}$, the oscillations practically dominate the perturbation to be captured; see Fig. 6. These WB results are in a good agreement with those reported in [2, §3.3.3].

It is also instructive to check whether the proposed WB scheme is capable of preserving the L^2-norm of the energy
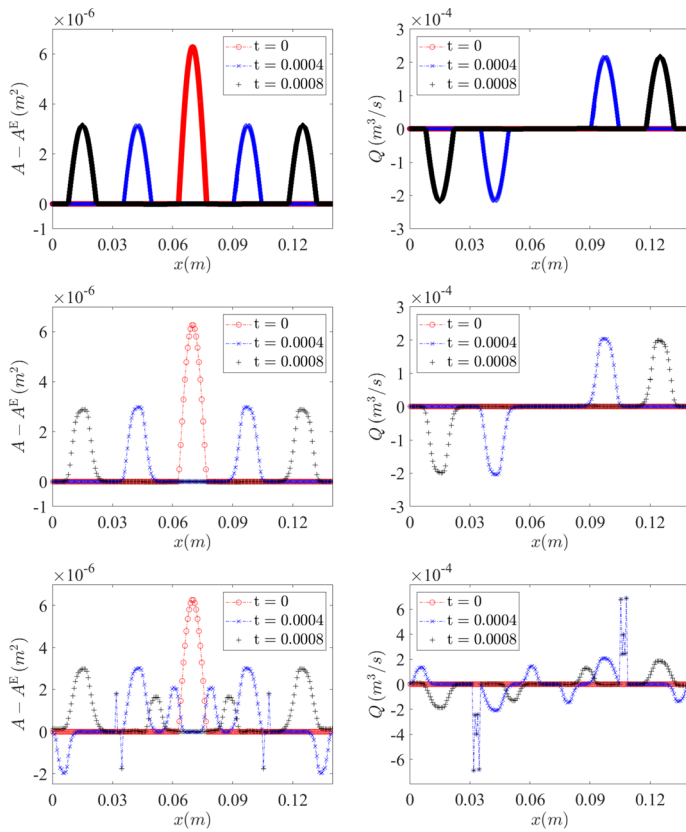
Fig. 5 Example 4, $\varepsilon = 10^{-3}$: Differences between the reference (top row), WB (middle row), and NWB (bottom row) solutions and the steady state at three different times
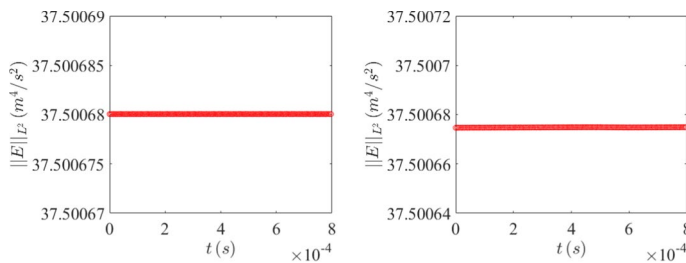
$$E = \frac{Q^2}{2A} + \frac{2\beta}{3}A^{\frac{3}{2}} - \beta A \sqrt{B}$$

for continuous solutions. Even though proving the energy stability property is out of reach, the results reported in Fig. 7 suggest that the energy is preserved in this example.

Our next goal is to compare the efficiency of the proposed WB scheme with its NWB counterpart. To this end, we perform a more thorough comparison between the WB and NWB schemes by taking into account additional computational cost of the WB scheme. We first measure the CPU time consumed by the WB scheme in computing the numerical solution (with $\varepsilon = 10^{-4}$) at the final time $t = 0.0008$ s on 200 uniform cells, and then refine the mesh in the NWB computations to 250 uniform cells, for which the same CPU time is consumed by the NWB scheme. The obtained results are plotted in Fig. 8 together with the reference solution. As one can clearly see, the WB scheme achieves a comparable resolution of the propagating waves despite using a coarser mesh and the WB
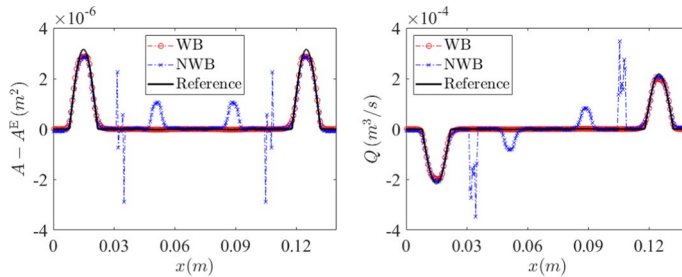
Fig. 6 Example 4: Same as in Fig. 5, but for $\varepsilon = 10^{-4}$

Fig. 7 Example 4: L^2-norm of the energy E for $\varepsilon = 10^{-4}$ (left) and 10^{-3} (right) as a function of time

solution is oscillation-free while the NWB solution contains quite large unphysical oscillations.

Finally, we verify the second order of accuracy of the proposed WB scheme. To this end, we slightly modify the initial data by making the initial perturbation of A^E smooth:

Fig. 8 Example 4, $\varepsilon = 10^{-4}$: Differences between the steady state and the following three solutions: the WB computed on 200 uniform cells, the NWB computed on 250 cells, and the reference ones

$$\overline{A}_j(0) = \begin{cases} \overline{A}_j^{\mathrm{E}}\left[1 + \varepsilon \cos^2\left(\frac{500\pi}{7}x_j\right)\right]^2 & \text{if } \in \left[\frac{9L}{20}, \frac{11L}{20}\right], \\ \overline{A}_j^{\mathrm{E}} & \text{otherwise}, \end{cases} \qquad \overline{Q}_j(0) \equiv 0,$$

and compute the solution at the time $t = 0.0004$ s on a sequence of meshes with 500, 1000, 2000, 4000, 8000, 16,000, and 32,000 uniform cells.

We then estimate the L^1-errors and the experimental convergence rates using the following Runge formulae, which are based on the solutions computed on the three consecutive uniform grids with the mesh sizes Δx, $2\Delta x$, and $4\Delta x$ and denoted by $(\cdot)^{\Delta x}$, $(\cdot)^{2\Delta x}$, and $(\cdot)^{4\Delta x}$, respectively:

$$\text{Error}(\Delta x) \approx \frac{\delta_{24}^2}{|\delta_{12} - \delta_{24}|}, \quad \text{Rate}(\Delta x) \approx \log_2\left(\frac{\delta_{24}}{\delta_{12}}\right).$$
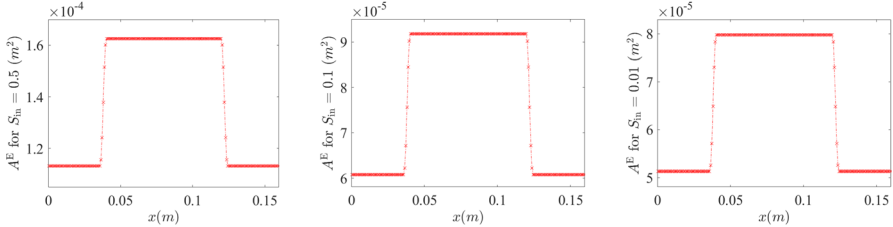
Here, $\delta_{12} := \|(\cdot)^{\Delta x} - (\cdot)^{2\Delta x}\|_{L^1}$ and $\delta_{24} := \|(\cdot)^{2\Delta x} - (\cdot)^{4\Delta x}\|_{L^1}$. The errors and corresponding rates for both A and Q with both $\varepsilon = 10^{-3}$ and 10^{-4} are reported in Table 2, where one can clearly see that convergence rates of the proposed WB scheme achieves the expected second order of accuracy on smooth solutions.

Table 2 Example 4: L^1-errors and experimental convergence rates

Δx	$\varepsilon = 10^{-3}$				$\varepsilon = 10^{-4}$			
	A		Q		A		Q	
	Error	Rate	Error	Rate	Error	Rate	Error	Rate
7/100, 000	1.05e−08	1.91	7.20e−07	1.91	1.05e−09	1.91	7.20e−08	1.91
7/200, 000	2.73e−09	2.00	1.88e−07	2.00	2.74e−10	2.00	1.87e−08	2.00
7/400, 000	6.81e−10	2.01	4.68e−08	2.01	6.84e−11	2.01	4.68e−09	2.01
7/800, 000	1.69e−10	2.01	1.16e−08	2.01	1.70e−11	2.01	1.16e−09	2.01
7/1, 600, 000	4.20e−11	2.01	2.88e−09	2.01	4.21e−12	2.01	2.88e−10	2.01

Table 3 Example 5: $\widehat{Q}$ and $\widehat{K}$ for different S_{in}

| S_{in}	$\widehat{Q}$	$\widehat{K}$
0.5	$9.513275470019762 \times 10^{-4}$	$2.9341289877866938 \times 10^{-2}$
0.1	$8.762209514474051 \times 10^{-5}$	$8.5417493720894352 \times 10^{-3}$
0.01	$7.078404140725565 \times 10^{-6}$	$6.5152635381013440 \times 10^{-3}$

Fig. 9 Example 5: Discrete steady state A^{E} for different S_{in}

3.2.2 Example 5—Perturbation of A for the aneurysm

In this example taken from [2, §5.3.1], we consider the "living-man" equilibrium with $\widehat{Q} \neq 0$ and the cross-sectional radius representing an aneurysm. Here, $B(x) = \pi r_0^2(x)$ and the cross-sectional radius $r_0(x)$ at rest is defined by

$$
r_0(x) = \begin{cases}
\tilde{r}, & x \in [0, x_1] \cup [x_4, L], \\
\tilde{r} + \frac{\Delta r}{2} \left[1 - \cos\left(\frac{x - x_1}{x_2 - x_1} \pi \right) \right], & x \in [x_1, x_2], \\
\tilde{r} + \Delta r, & x \in [x_2, x_3], \\
\tilde{r} + \frac{\Delta r}{2} \left[1 + \cos\left(\frac{x - x_3}{x_4 - x_3} \pi \right) \right], & x \in [x_3, x_4],
\end{cases}
\tag{3.16}
$$

where $\tilde{r} = 4 \times 10^{-3}$ m, $\Delta r = 10^{-3}$ m, $L = 0.16$ m, $x_1 = 9L/40$, $x_2 = L/4$, $x_3 = 3L/4$, and $x_4 = 33L/40$.

We first compute the discrete steady state solution with $\overline{Q}_j^{\text{E}} \equiv \widehat{Q} = Q_{\text{in}}$ and $K_j^{\text{E}} \equiv \widehat{K}$ with the value $\widehat{K}$ as well as the cell averages $\overline{A}_j^{\text{E}}$ obtained using (3.10)–(3.15). The values $\widehat{Q}$ and $\widehat{K}$ for different Shapiro numbers S_{in} are presented in Table 3 and the corresponding discrete steady states A^{E} are plotted in Fig. 9. We then set the perturbed initial data as follows:

$$
\overline{A}_j(0) = \begin{cases}
\overline{A}_j^{\text{E}} + \varepsilon^2 \pi \cos^2\left(\frac{125\pi}{2} x_j \right) & \text{if } x_j \in \left[\frac{45L}{100}, \frac{55L}{100} \right], \\
\overline{A}_j^{\text{E}} & \text{otherwise},
\end{cases}
\qquad \overline{Q}_j(0) = \widehat{Q},
\tag{3.17}
$$

which contains a small perturbation of A^{E} as we take $\varepsilon = 5 \times 10^{-5}$.
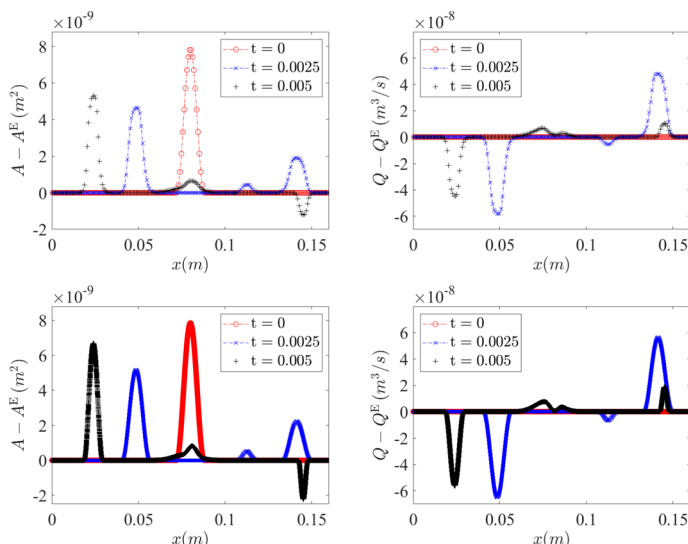
In this example, the boundary conditions are prescribed as follows. At $x = 0$, we set $A^-_{j_\ell - \frac{1}{2}} = A_{\text{in}}$ and $Q^-_{j_\ell - \frac{1}{2}} = Q_{\text{in}}$, and then evaluate $K^-_{j_\ell - \frac{1}{2}}$ using (2.2) and (2.3) with $\hat{x} = x_{j_\ell - \frac{1}{2}}$, which gives

$$K^-_{j_\ell - \frac{1}{2}} = \frac{Q^2_{\text{in}}}{A^-_{j_\ell - \frac{1}{2}}} + \frac{\beta}{3}\left(A^-_{j_\ell - \frac{1}{2}}\right)^{\frac{3}{2}}.$$
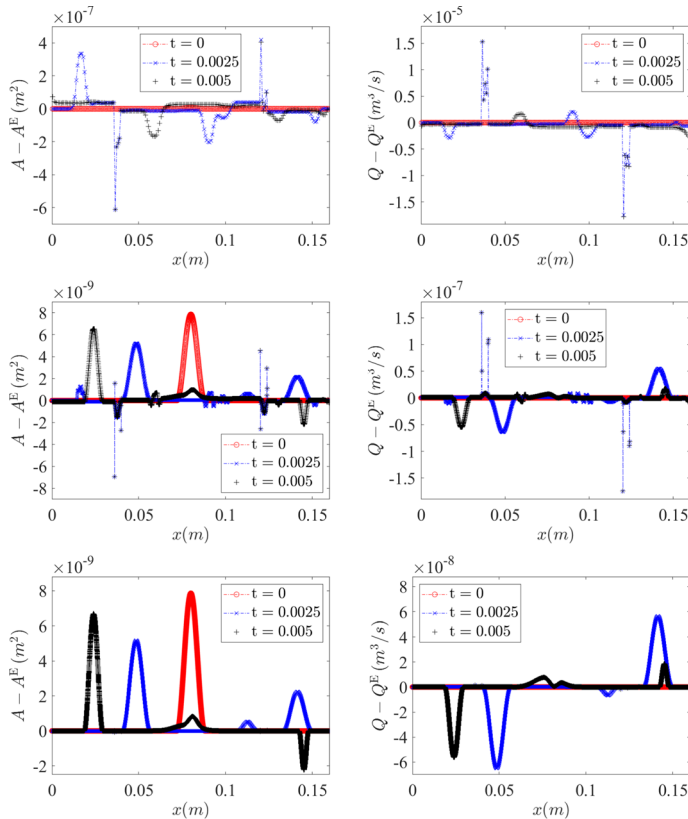
After that, we obtain the point values $Q^+_{j_\ell - \frac{1}{2}}$, $Q^-_{j_\ell + \frac{1}{2}}$, $K^+_{j_\ell - \frac{1}{2}}$ and $K^-_{j_\ell + \frac{1}{2}}$ using (3.5) and (3.7), and compute $A^+_{j_\ell - \frac{1}{2}}$ by solving the nonlinear equation (2.22) for $j = j_\ell$ and $i = +$.

At $x = L$, we set $A^+_{j_r + \frac{1}{2}} = A_{\text{out}}$, use the free boundary for Q which results in $Q^\pm_{j_r + \frac{1}{2}} = Q_{j_r}$, and compute $K^+_{j_r + \frac{1}{2}}$ by (2.22). The latter point value is utilized to compute the slope $(K_x)_{j_r}$ as in (3.6), which is then used to calculate the values $K^+_{j_r - \frac{1}{2}}$ and $K^-_{j_r + \frac{1}{2}}$ as in (3.8). Finally, $A^-_{j_r + \frac{1}{2}}$ is computed by solving the nonlinear equation (2.22) for $j = j_r$ and $i = -$.

We compute the numerical solutions by both the WB and NWB schemes on 200 uniform cells until the final time $t = 0.005$ s. The differences between the perturbed solutions and the corresponding steady states for $S_{\text{in}} = 0.5, 0.1$ and 0.01 are presented in the top rows in Figs. 10, 11, 12, 13, 14 and 15. As one can see, the WB scheme is capable of accurately capturing the perturbation (see the reference solutions shown in the bottom rows in Figs. 10, 12, and 14), while the NWB scheme fails as the

Fig. 10 Example 5, $S_{\text{in}} = 0.5$: Differences between the WB (top row) and reference (bottom row) solutions and the steady state at three different times
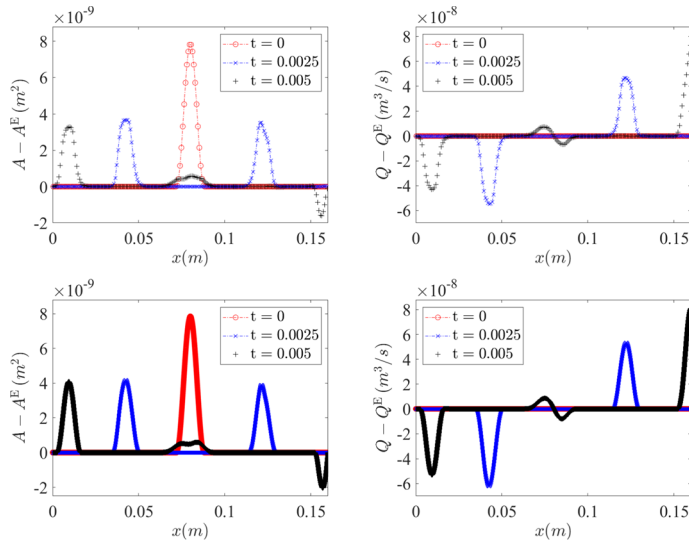
Fig. 11 Example 5, $S_{\text{in}} = 0.5$: Differences between the solutions computed by the NWB scheme on 200 (top row), 2000 (middle row), and 2000 (bottom row) uniform cells, and the steady state at three different times

magnitude of the artificial waves produced by the NWB scheme is way too large. In order to further investigate the performance of the NWB scheme, we refine the mesh and compute the NWB results using 2000 uniform cells. At this resolution, the perturbation is captured, but the magnitude of oscillations is still comparable or even higher than the size of the perturbation, especially for the large values of S_{in}; see the second rows in Figs. 11, 13, and 15 . We therefore use even finer mesh with 20,000 uniform cells and then the NWB results are oscillation-free; see the bottom rows in Figs. 11, 13, and 15 . However, as expected, the efficiency of the NWB scheme is extremely low, which clearly demonstrates the advantage of the WB scheme.

3.3 Numerical test for the system (1.4)–(1.5)

In this section, we apply the studied WB and NWB CU scheme to the system (1.4)–(1.5) with both $\alpha \neq 0$ and $\beta \neq 0$.

Fig. 12 Example 5: Same as in Fig. 10, but for $S_{\text{in}} = 0.1$

3.3.1 Example 6—Perturbation of A for the aneurysm

This example is a modification of Example 5 with an added friction term with
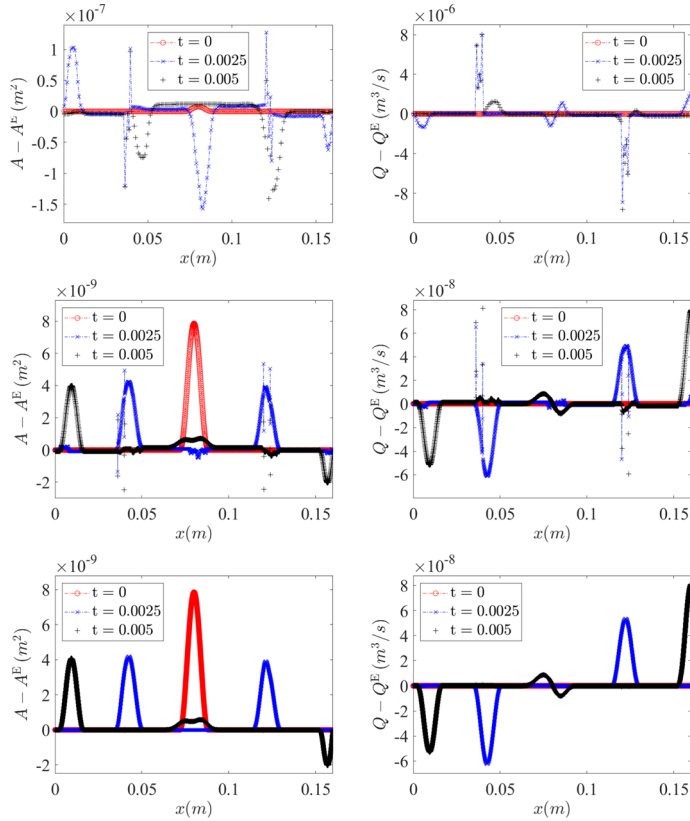
$$\alpha(x) = \frac{11\pi}{70{,}000}\left[1 + 0.1\sin\left(\frac{25\pi}{2}x\right)\right].$$

As in Example 5, $\beta = 5 \times 10^6/53\sqrt{\pi}$ and the cross-section function $B(x)$ is defined by (3.16). We consider three cases with the values of $S_{\text{in}}, \widehat{Q}$ and $\widehat{K}$ given in Table 3.

We first take a steady-state solution given in terms of $Q^{\text{E}}(x) \equiv \widehat{Q}$ and $K^{\text{E}}(x) \equiv \widehat{K}$, and compute the corresponding cells averages $\overline{A}_j^{\text{E}}$ as follows. We begin with computing the point value $A_{j_\ell - \frac{1}{2}}$ by solving the nonlinear equation (2.2) with $Q_{j_\ell - \frac{1}{2}} = \widehat{Q}$, $K_{j_\ell - \frac{1}{2}} = \widehat{K}$ and $R_{j_\ell - \frac{1}{2}} = S_{j_\ell - \frac{1}{2}} = 0$. Equipped with $A_{j_\ell - \frac{1}{2}}$, we proceed with computing the cell average $\overline{A}_{j_\ell}^{\text{E}}$ by solving the nonlinear equation (2.2), which for $A = \overline{A}_{j_\ell}^{\text{E}}$ reads as

$$\frac{\widehat{Q}^2}{\overline{A}_{j_\ell}^{\text{E}}} + \frac{\beta}{3}\left(\overline{A}_{j_\ell}^{\text{E}}\right)^{\frac{3}{2}} + R_{j_\ell} + S_{j_\ell} = \widehat{K}, \tag{3.18}$$

where R_{j_ℓ} and S_{j_ℓ} are given by (2.17) and (2.18), respectively. We then obtain $\overline{A}_{j+1}^{\text{E}}$ for $j \geq j_\ell$ recursively by solving (2.2) for $A = \overline{A}_{j+1}^{\text{E}}$ with $R = R_{j+1}$ and $S = S_{j+1}$:
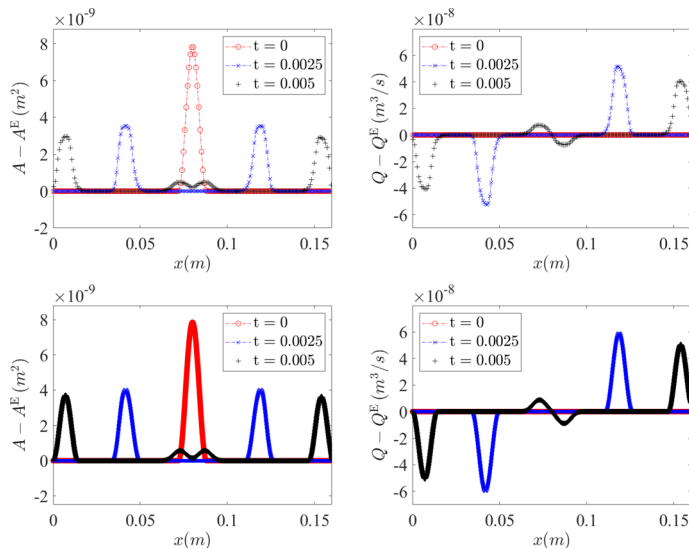
Fig. 13 Example 5: Same as in Fig. 11, but for $S_{\text{in}} = 0.1$

$$\frac{\widehat{Q}^2}{\overline{A}_{j+1}^{\text{E}}} + \frac{\beta}{3}\left(\overline{A}_{j+1}^{\text{E}}\right)^{\frac{3}{2}} + R_j - \frac{\beta}{3}\left(\overline{A}_j^{\text{E}} + \overline{A}_{j+1}^{\text{E}} + \sqrt{\overline{A}_j^{\text{E}}\,\overline{A}_{j+1}^{\text{E}}}\right)\left(\sqrt{B_{j+1}} - \sqrt{B_j}\right)$$

$$+ S_j + \frac{\widehat{Q}\Delta x}{2}\left[\frac{\alpha(x_{j+1})}{\overline{A}_{j+1}^{\text{E}}} + \frac{\alpha(x_j)}{\overline{A}_j^{\text{E}}}\right] = \widehat{K}, \quad j = j_\ell, \dots, j_r - 1.$$

$$(3.19)$$

Here, the global variables R_j and S_j are also defined recursively by (2.15)–(2.18). We numerically solve the nonlinear equations in (3.18) and (3.19) using the same initial guess as in Example 5.

The obtained steady states for different values of S_{in} are plotted in Fig. 16. As one can see, the steady states are different from those obtained in the frictionless case; compare with Fig. 9. Next we add a small perturbation and consider the initial data (3.17) and the same boundary conditions as in Example 5 with the only exception
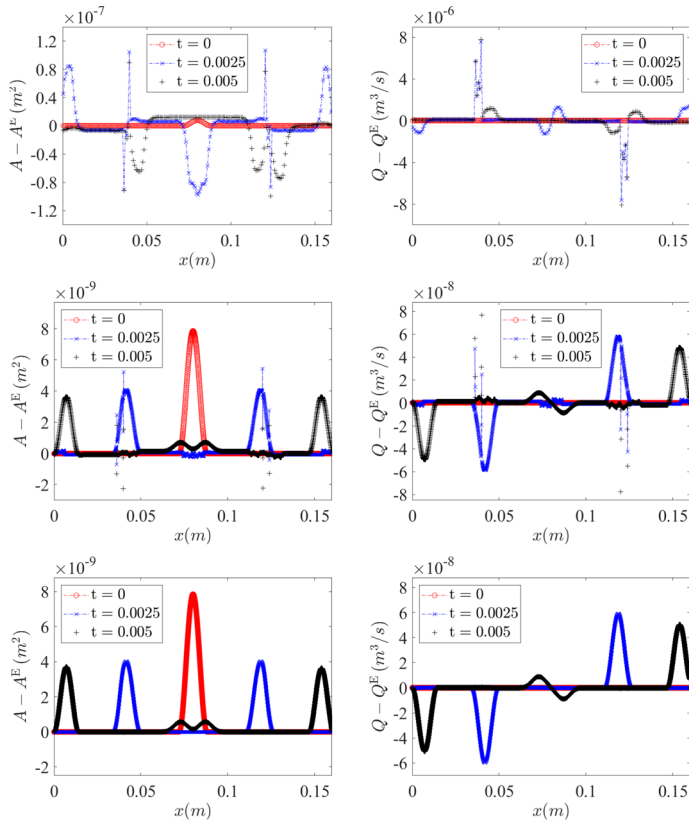
Fig. 14 Example 5: Same as in Figs. 10 and 12 , but for $S_{\text{in}} = 0.01$

that we now do not prescribe the value A_{out}. Instead, we compute $A^+_{j_r+\frac{1}{2}}$ by solving the nonlinear equation (2.22) for $j = j_r$ and $i = +$ with $Q_{j_r+\frac{1}{2}} = \widehat{Q}$ and $K_{j_r+\frac{1}{2}} = \widehat{K}$.
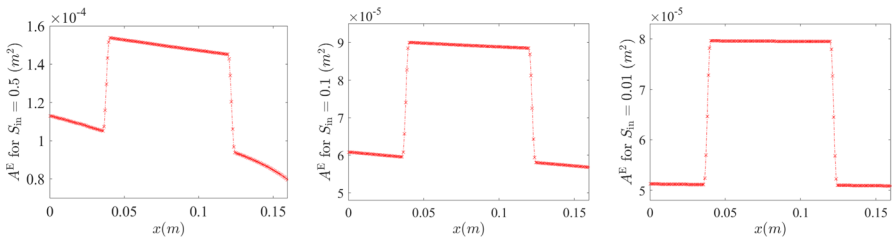
We compute the numerical solution by both the WB and NWB schemes until the final time $t = 0.005$ s. The differences between the perturbed solutions and the corresponding steady states are presented in Figs. 17, 18, 19, 20, 21 and 22. One can observe that, as in Example 5, the WB scheme can capture the small perturbation accurately, while the NWB scheme fails even in the presence of the friction term.

4 Conclusion

In this paper, we have developed a new second-order well-balanced (WB) central-upwind (CU) scheme for several one-dimensional blood flow models. In order to achieve this goal, we have extended the flux globalization approach to the studied models and implemented it to develop the WB CU scheme which can preserve both "man-at-eternal-rest" (zero-velocity) and "living-man" (non-zero velocity) steady-state solutions. We have tested the proposed WB CU scheme on a number of numerical examples and demonstrated that it clearly outperforms its non-well-balanced counterpart despite an increased computational cost per time step.
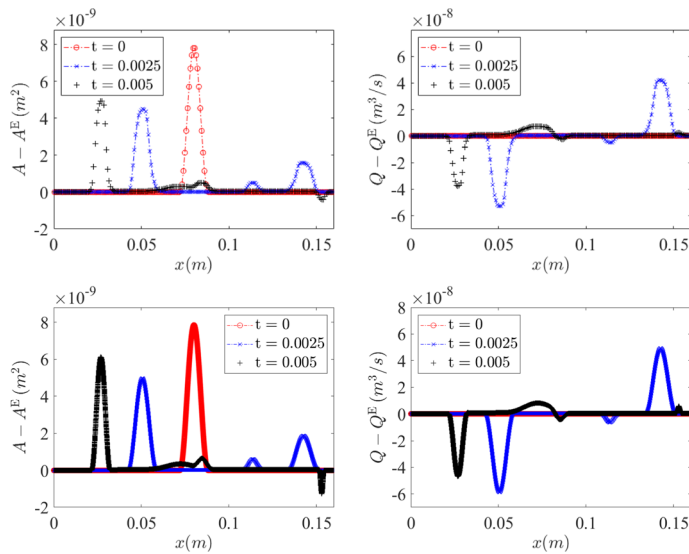
**Fig. 15** Example 5: Same as in Figs. 11 and 13 , but for $S_{\text{in}} = 0.01$

Fig. 16 Example 6: Discrete steady state A^{E} for different S_{in}

Solving (2.22) by Newton's method

In order to numerically solve (2.22), we first rewrite it in the following form:

Fig. 17 Example 6, $S_{in} = 0.5$: Differences between the WB (top row) and reference (bottom row) solutions and the steady state at three different times

$$\mathcal{F}(A^i_{j+\frac{1}{2}}) := \frac{(Q^i_{j+\frac{1}{2}})^2}{A^i_{j+\frac{1}{2}}} + \frac{\beta}{3}(A^i_{j+\frac{1}{2}})^{\frac{3}{2}} + R_{j+\frac{1}{2}} + S_{j+\frac{1}{2}} - K^i_{j+\frac{1}{2}} = 0, \qquad (A.1)$$

which we consider for positive $A^i_{j+\frac{1}{2}}$ only. It is easy to show that this function admits it minimum at the point
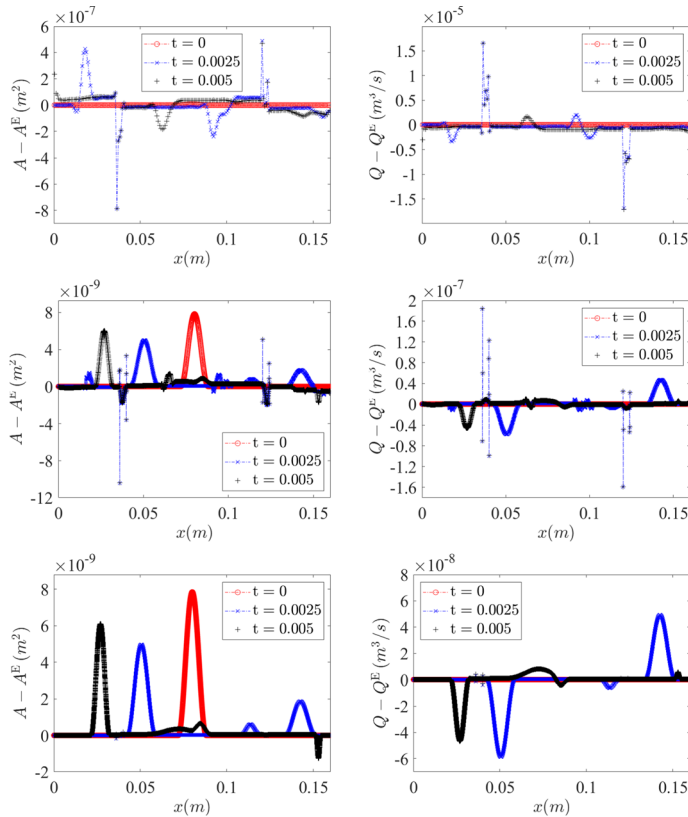
$$A^i_{j+\frac{1}{2}} = \check{A}^i_{j+\frac{1}{2}} := \left[\frac{2}{\beta}(Q^i_{j+\frac{1}{2}})^2\right]^{\frac{2}{5}},$$

and therefore, three possible cases are to be considered.

Case 1: $\mathcal{F}(\check{A}^i_{j+\frac{1}{2}}) > 0$. This case is unphysical, but may occur in the transcritical case due to the numerical errors. In this case, (A.1) has no positive solutions and instead of solving (A.1), we locally apply the minmod reconstruction (in either the cell C_j if $i = -$ in (A.1) or C_{j+1} if $i = +$ in (A.1)) directly to A.

Case 2: $\mathcal{F}(\check{A}^i_{j+\frac{1}{2}}) = 0$. This is a transcritical case, in which the only positive solution of (A.1) is $A^i_{j+\frac{1}{2}} = \check{A}^i_{j+\frac{1}{2}}$.

Case 3: $\mathcal{F}(\check{A}^i_{j+\frac{1}{2}}) < 0$. This is generic case, in which (A.1) has two positive solutions: a supercritical (with $A^i_{j+\frac{1}{2}} < \check{A}^i_{j+\frac{1}{2}}$) and a subcritical (with $A^i_{j+\frac{1}{2}} > \check{A}^i_{j+\frac{1}{2}}$) one. In all of the studied numerical examples, the blood flow is subcritical and hence we find the subcritical root using Newton's method directly applied to (A.1). As the

Fig. 18 Example 6, $S_{in} = 0.5$: Differences between the solutions computed by the NWB scheme on 200 (top row), 2000 (middle row), and 2000 (bottom row) uniform cells, and the steady state at three different times

function $\mathcal{F}$ is convex, the use of any initial guess larger than $\check{A}^i_{j+\frac{1}{2}}$ will ensure Newton's method to converge to the subcritical root. In the numerical examples reported in Sect. 3, we have taken the following initial guesses: A_{ref} (specified after Eq. (3.1)) in Examples 1–3 and A_{in} (given in (3.15)) in Examples 4–6.
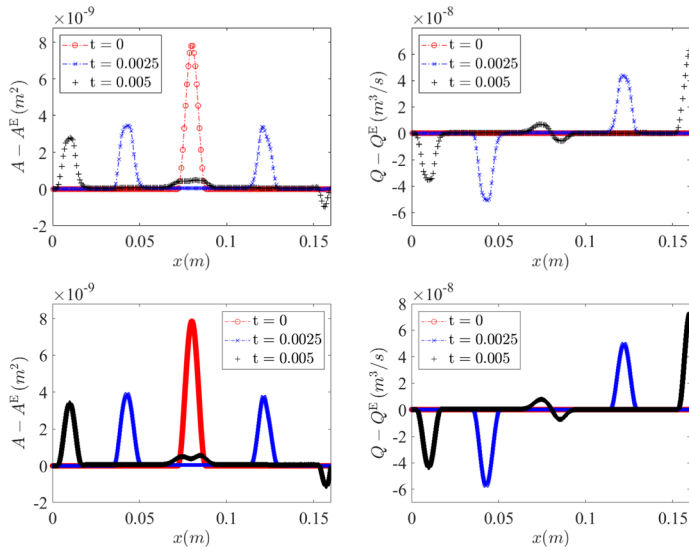
Non-well-balanced central-upwind scheme

In this appendix, we briefly describe the NWB CU scheme for the system (1.4), (1.5), which we have used in the numerical examples reported in Sect. 3.
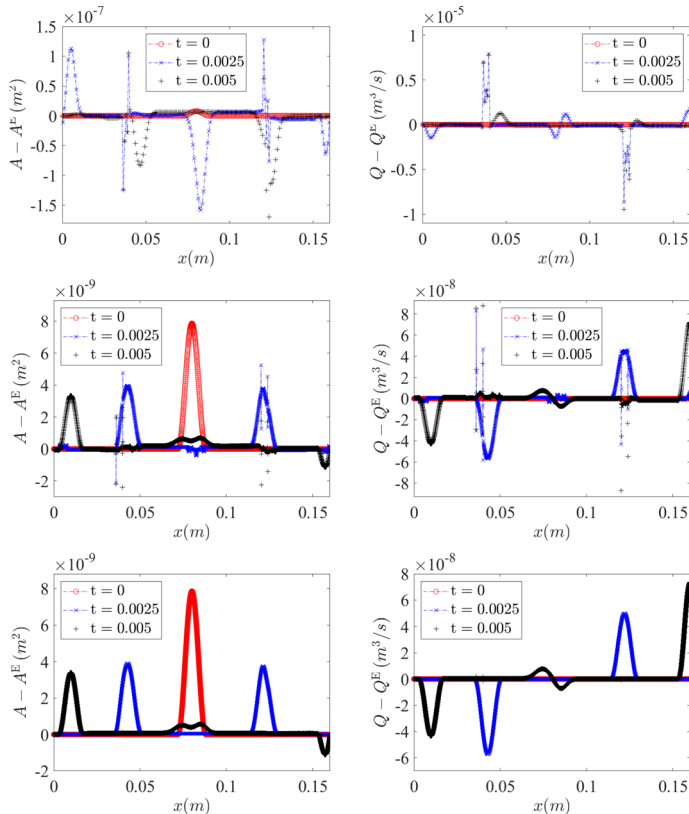
We first write the system of balance laws (1.4), (1.5) in the vector form

$$U_t + \mathcal{F}(U)_x = S(U),$$
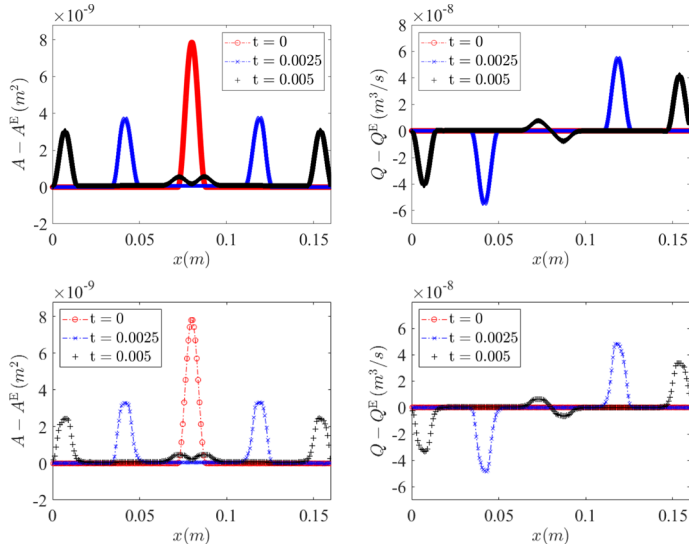
with

Fig. 19 Example 6: Same as in Fig. 17, but for $S_{\mathrm{in}} = 0.1$

**Fig. 20** Example 6: Same as in Fig. 18, but for $S_{\mathrm{in}} = 0.1$

Fig. 21 Example 6: Same as in Figs. 17 and 19, but for $S_{in} = 0.01$

$$\mathcal{F}(U) = \begin{pmatrix} Q \\ \dfrac{Q^2}{A} + \dfrac{\beta}{3} A^{\frac{3}{2}} \end{pmatrix}, \quad S(U) = \begin{pmatrix} 0 \\ \beta A \left(\sqrt{B} \right)_x - \alpha \dfrac{Q}{A} \end{pmatrix},$$

and then evolve the cell averages $\overline{U}_j$ by solving the following system of ODEs:

$$\frac{d\overline{U}_j}{dt} = -\frac{\mathcal{H}_{j+\frac{1}{2}} - \mathcal{H}_{j-\frac{1}{2}}}{\Delta x} + \beta \overline{A}_j \frac{\sqrt{B_{j+\frac{1}{2}}} - \sqrt{B_{j-\frac{1}{2}}}}{\Delta x} - \alpha_j \frac{\overline{Q}_j}{\overline{A}_j}.$$
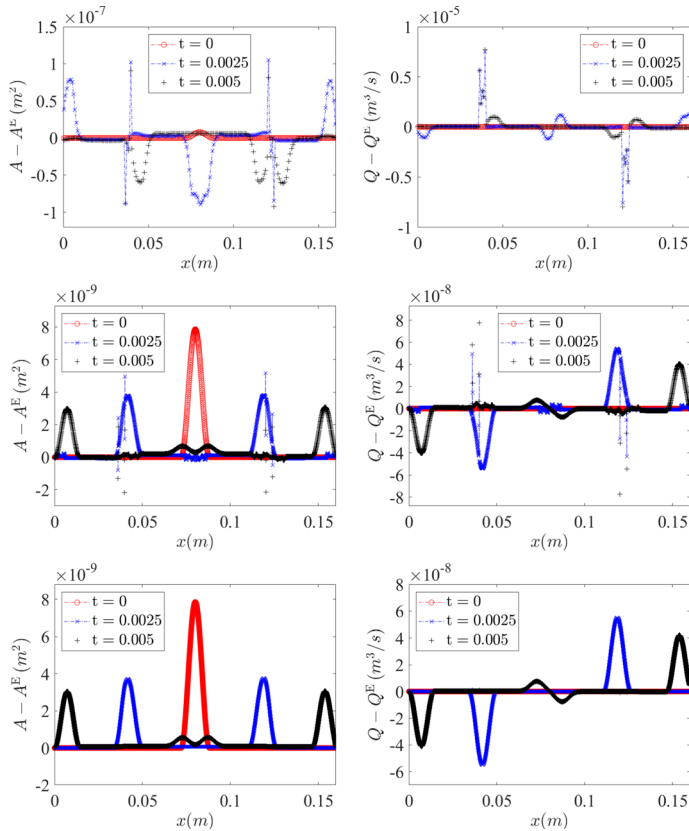
Here, $\mathcal{H}_{j+\frac{1}{2}}$ are the CU numerical fluxes

$$\mathcal{H}_{j+\frac{1}{2}} = \frac{a^+_{j+\frac{1}{2}} \mathcal{F}^-_{j+\frac{1}{2}} - a^-_{j+\frac{1}{2}} \mathcal{F}^+_{j+\frac{1}{2}}}{a^+_{j+\frac{1}{2}} - a^-_{j+\frac{1}{2}}} + \frac{a^+_{j+\frac{1}{2}} a^-_{j+\frac{1}{2}}}{a^+_{j+\frac{1}{2}} - a^-_{j+\frac{1}{2}}} \left(U^+_{j+\frac{1}{2}} - U^-_{j+\frac{1}{2}} - \delta U_{j+\frac{1}{2}} \right) \quad \text{(B.1)}$$

with $\delta U_{j+\frac{1}{2}}$ given by (2.8) with

$$U^*_{j+\frac{1}{2}} = \frac{a^+_{j+\frac{1}{2}} U^+_{j+\frac{1}{2}} - a^-_{j+\frac{1}{2}} U^-_{j+\frac{1}{2}} - \left\{ \mathcal{F}(U^+_{j+\frac{1}{2}}) - \mathcal{F}(U^-_{j+\frac{1}{2}}) \right\}}{a^+_{j+\frac{1}{2}} - a^-_{j+\frac{1}{2}}}, \quad \text{(B.2)}$$

and $a^\pm_{j+\frac{1}{2}}$ given by (2.9). The point values $U^\pm_{j+\frac{1}{2}}$, which are used in (B.1), (2.8), (B.2) and (2.9), are now computed by applying the minmod reconstruction (2.19)–(2.21) applied to U rather than to F.

Fig. 22 Example 6: Same as in Fig. 18 and 20, but for $S_{\text{in}} = 0.01$

Boundary conditions for the non-well-balanced scheme

In Examples 1–3 reported in Sect. 3.1, we have prescribed the Dirichlet boundary conditions, namely, the values of A and Q at the left $(A^-_{j_\ell-\frac{1}{2}}, Q^-_{j_\ell-\frac{1}{2}})$ and right $(A^+_{j_r+\frac{1}{2}}, Q^+_{j_r+\frac{1}{2}})$ endpoints of the computational domain. We then use these values to compute the slopes of A in the cells C_{j_ℓ} and C_{j_r} as follows:

$$(A_x)_{j_\ell} = \text{minmod}\left(\frac{\overline{A}_{j_\ell} - A^-_{j_\ell-\frac{1}{2}}}{\Delta x/2}, \frac{\overline{A}_{j_\ell+1} - \overline{A}_{j_\ell}}{\Delta x}\right),$$

$$(A_x)_{j_r} = \text{minmod}\left(\frac{\overline{A}_{j_r} - \overline{A}_{j_r-1}}{\Delta x}, \frac{A^+_{j_r+\frac{1}{2}} - \overline{A}_{j_r}}{\Delta x/2}\right).$$

We then use these slopes to compute the corresponding boundary point values of A:

$$A^+_{j_\ell - \frac{1}{2}} = \overline{A}_{j_\ell} - \frac{\Delta x}{2}(A_x)_{j_\ell}, \quad A^-_{j_r + \frac{1}{2}} = \overline{A}_{j_r} + \frac{\Delta x}{2}(A_x)_{j_r}.$$

The slopes of Q and the boundary point values $Q^+_{j_\ell - \frac{1}{2}}$ and $Q^-_{j_r + \frac{1}{2}}$ are computed similarly.

In Examples 4 reported in Sect. 3.2, we have used free boundary conditions, namely, we set

$$A^\pm_{j_\ell - \frac{1}{2}} = \overline{A}_{j_\ell}, \quad A^\pm_{j_r + \frac{1}{2}} = \overline{A}_{j_r}, \quad Q^\pm_{j_\ell - \frac{1}{2}} = \overline{Q}_{j_\ell}, \quad Q^\pm_{j_r + \frac{1}{2}} = \overline{Q}_{j_r}.$$

In Example 5 reported in Sect. 3.2, the boundary conditions are prescribed as in Examples 1–3 except for Q at the right endpoint of the computational domain, which is set to $Q^\pm_{j_r + \frac{1}{2}} = \overline{Q}_{j_r}$.

In Example 6 reported in Sect. 3.3, the boundary conditions are the same as in Example 5 with the only exception that $A^+_{j_r + \frac{1}{2}}$ is now computed by solving the nonlinear equation (2.22) for $j = j_r$ and $i = +$ with $Q_{j_r + \frac{1}{2}} = \widehat{Q}$ and $K_{j_r + \frac{1}{2}} = \widehat{K}$.

References

1. Bollermann, A., Noelle, S., Lukáčová-Medviďová, M.: Finite volume evolution Galerkin methods for the shallow water equations with dry beds. Commun. Comput. Phys. **10**, 371–404 (2011)
2. Britton, J., Xing, Y.: Well-balanced discontinuous Galerkin methods for the one-dimensional blood flow through arteries model with man-at-eternal-rest and living-man equilibria. Comput. Fluids **203**, 104493 (2020). (**32**)
3. Cheng, Y., Chertock, A., Herty, M., Kurganov, A., Wu, T.: A new approach for designing moving-water equilibria preserving schemes for the shallow water equations. J. Sci. Comput. **80**, 538–554 (2019)
4. Chertock, A., Cui, S., Kurganov, A., Özcan, ŞN., Tadmor, E.: Well-balanced schemes for the Euler equations with gravitation: conservative formulation using global fluxes. J. Comput. Phys. **358**, 36–52 (2018)
5. Chertock, A., Herty, M., Özcan, ŞN.: Well-balanced central-upwind schemes for 2×2 systems of balance laws. In: Klingenberg, C., Westdickenberg, M. (eds.) Theory, Numerics and Applications of Hyperbolic Problems. I, vol. 236 of Springer Proc. Math. Stat., pp. 345–361. Springer, Cham (2018)
6. Chertock, A., Kurganov, A., Liu, X., Liu, Y., Wu, T.: Well-balancing via flux globalization: Applications to shallow water equations with wet/dry fronts. J. Sci. Comput. **90** (2022). (**Published online on November 20, (2021)**))
7. Del Grosso, A., Chalons, C.: Second-order well-balanced Lagrange-projection schemes for blood flow equations. Calcolo **58**, 43 (2021)
8. Delestre, O., Lagrée, P.-Y.: A 'well-balanced' finite volume scheme for blood flow simulation. Int. J. Numer. Methods Fluids **72**, 177–205 (2013)
9. Formaggia, L., Lamponi, D., Quarteroni, A.: One-dimensional models for blood flow in arteries. J. Eng. Math. **47**, 251–276 (2003)
10. Ghitti, B., Berthon, C., Le, M.H., Toro, E.F.: A fully well-balanced scheme for the 1D blood flow equations with friction source term. J. Comput. Phys. **421**, 109750 (2020)

11. Gottlieb, S., Ketcheson, D., Shu, C.-W.: Strong Stability Preserving Runge–Kutta and Multistep Time Discretizations. World Scientific Publishing Co. Pte. Ltd., Hackensack (2011)
12. Gottlieb, S., Shu, C.-W., Tadmor, E.: Strong stability-preserving high-order time discretization methods. SIAM Rev. **43**, 89–112 (2001)
13. Kurganov, A.: Finite-volume schemes for shallow-water equations. Acta Numer. **27**, 289–351 (2018)
14. Kurganov, A., Lin, C.-T.: On the reduction of numerical dissipation in central-upwind schemes. Commun. Comput. Phys. **2**, 141–163 (2007)
15. Kurganov, A., Liu, Y., Zeitlin, V.: A well-balanced central-upwind scheme for the thermal rotating shallow water equations. J. Comput. Phys. **411**, 109414 (2020)
16. Kurganov, A., Noelle, S., Petrova, G.: Semidiscrete central-upwind schemes for hyperbolic conservation laws and Hamilton–Jacobi equations. SIAM J. Sci. Comput. **23**, 707–740 (2001)
17. Kurganov, A., Petrova, G.: A second-order well-balanced positivity preserving central-upwind scheme for the Saint-Venant system. Commun. Math. Sci. **5**, 133–160 (2007)
18. Kurganov, A., Tadmor, E.: New high-resolution semi-discrete central schemes for Hamilton–Jacobi equations. J. Comput. Phys. **160**, 720–742 (2000)
19. Lie, K.-A., Noelle, S.: On the artificial compression method for second-order nonoscillatory central difference schemes for systems of conservation laws. SIAM J. Sci. Comput. **24**, 1157–1174 (2003)
20. Müller, L., Toro, E.F.: Well-balanced high-order solver for blood flow in networks of vessels with variable properties. Int. J. Numer. Methods Biomed. Eng. **29**, 1388–1411 (2013)
21. Nessyahu, H., Tadmor, E.: Nonoscillatory central differencing for hyperbolic conservation laws. J. Comput. Phys. **87**, 408–463 (1990)
22. Sherwin, S.J., Formaggia, L., Peiró, J., Franke, V.: Computational modelling of 1D blood flow with variable mechanical properties and its application to the simulation of wave propagation in the human arterial system. Int. J. Numer. Methods Fluids **43**, 673–700 (2003)
23. Sweby, P.K.: High resolution schemes using flux limiters for hyperbolic conservation laws. SIAM J. Numer. Anal. **21**, 995–1011 (1984)
24. Toro, E.F.: Brain venous haemodynamics, neurological diseases and mathematical modelling. A review. Appl. Math. Comput. **272**, 542–579 (2016)